Chang LJ, Ganem D, Varmus HE. 1990. Mechanism of translation of the hepadnaviral polymerase (P) gene. Proc Natl Acad Sci U S A 87:5158–5162.

Dandri M, Locarnini S. 2012. New insight in the pathobiology of hepatitis B virus infection. Gut 61:16–17.

Dane DS, Cameron CH, Briggs M. 1970. Virus-like particles in serum of patients with Australia-antigen-associated hepatitis. Lancet 1:695–698.

Dejean A, Bougueleret L, Grzeschik KH, Tiollais P. 1986. Hepatitis B virus DNA integration in a sequence homologous to v-erb-A and steroid receptor genes in a hepatocellular carcinoma. Nature 322:70–72.

Ezzikouri S, Kitab B, Rebbani K, Marchio A, Wain-Hobson S, Dejean A, Vartanian JP, Pineau P, Benjelloun S. 2013. Polymorphic APOBEC3 modulates chronic hepatitis B in Moroccan population. J Viral Hepat 20:678–686.

Ganem D. 1991. Assembly of hepadnaviral virions and subviral particles. Curr Top Microbiol Immunol 168:61–83.

Gripon P, Diot C, Theze N, Fourel I, Loreal O, Brechot C, Guguen-Guillouzo C. 1988. Hepatitis B virus infection of adult human hepatocytes cultured in the presence of dimethyl sulfoxide. J Virol 62:4136–4143.

Gripon P, Le Seyec J, Rumin S, Guguen-Guillouzo C. 1995. Myristylation of the hepatitis B virus large surface protein is essential for viral infectivity. Virology 213:292–299.

Gripon P, Rumin S, Urban S, Le Seyec J, Glaise D, Cannie I, Guyomard C, Lucas J, Trepo C, Guguen-Guillouzo C. 2002. Infection of a human hepatoma cell line by hepatitis B virus. Proc Natl Acad Sci U S A 99:15655–15660.

Gripon P, Cannie I, Urban S. 2005. Efficient inhibition of hepatitis B virus infection by acylated peptides derived from the large viral surface protein. J Virol 79:1613–1622.

Hao Z, Zheng L, Kluwe L, Huang W. 2012. Ferritin light chain and squamous cell carcinoma antigen 1 are coreceptors for cellular attachment and entry of hepatitis B virus. Int J Nanomedicine 7:827–834.

Hartmann-Stuhler C, Prange R. 2001. Hepatitis B virus large envelope protein interacts with gamma2-adaptin, a clathrin adaptor-related protein. J Virol 75:5343–5351.

Henry M, Guetard D, Suspene R, Rusniok C, Wain-Hobson S, Vartanian JP. 2009. Genetic editing of HBV DNA by monodomain human APOBEC3 cytidine deaminases and the recombinant nature of APOBEC3G. PLoS ONE 4:e4277.

Hoofnagle JH, Doo E, Liang TJ, Fleischer R, Lok AS. 2007. Management of hepatitis B: Summary of a clinical research workshop. Hepatology 45:1056–1075.

Hu W, Wang X, Ding X, Li Y, Zhang X, Xie P, Yang J, Wang S. 2012. MicroRNA-141 represses HBV replication by targeting PPARA. PLoS ONE 7:e34165.

Kann M, Sodeik B, Vlachou A, Gerlich WH, Helenius A. 1999. Phosphorylation-dependent binding of hepatitis B virus core particles to the nuclear pore complex. J Cell Biol 145:45–55.

Kullak-Ublick GA, Stieger B, Hagenbuch B, Meier PJ. 2000. Hepatic transport of bile salts. Semin Liver Dis 20:273–292.

Kuroki K, Eng F, Ishikawa T, Turck C, Harada F, Ganem D. 1995. gp180, a host cell glycoprotein that binds duck hepatitis B virus particles, is encoded by a member of the carboxypeptidase gene family. J Biol Chem 270:15022–15028.

Lazar C, Macovei A, Petrescu S, Branza-Nichita N. 2012. Activation of ERAD pathway by human hepatitis B virus modulates viral and subviral particle production. PLoS ONE 7:e34169.

Le Seyec J, Chouteau P, Cannie I, Guguen-Guillouzo C, Gripon P. 1998. Role of the pre-S2 domain of the large envelope protein in hepatitis B virus assembly and infectivity. J Virol 72: 5573–5578.

Lee WM. 1997. Hepatitis B virus infection. N Engl J Med 337: 1733–1745.

Leistner CM, Gruen-Bernhard S, Glebe D. 2008. Role of glycosaminoglycans for binding and infection of hepatitis B virus. Cell Microbiol 10:122–133.

Levrero M, Pollicino T, Petersen J, Belloni L, Raimondo G, Dandri M. 2009. Control of cccDNA function in hepatitis B virus infection. J Hepatol 51:581–592.

Li HC, Huang EY, Su PY, Wu SY, Yang CC, Lin YS, Chang WC, Shih C. 2010. Nuclear export and import of human hepatitis B virus capsid protein and particles. PLoS Pathog 6:e1001162.

Li C, Wang Y, Wang S, Wu B, Hao J, Fan H, Ju Y, Ding Y, Chen L, Chu X, Liu W, Ye X, Meng S. 2013. Hepatitis B virus mRNA-mediated miR-122 inhibition upregulates PTTG1-binding protein, which promotes hepatocellular carcinoma tumor growth and cell invasion. J Virol 87:2193–2205.

Liang TJ. 2009. Hepatitis B: The virus and disease. Hepatology 49: S13–S21.

Lindsay MA. 2008. microRNAs and the immune response. Trends Immunol 29:343–351.

Liu C, Mason WS, Burch JB. 1994. Identification of factor-binding sites in the duck hepatitis B virus enhancer and in vivo effects of enhancer mutations. J Virol 68:2286–2296.

Liu WH, Yeh SH, Chen PJ. 2011. Role of microRNAs in hepatitis B virus replication and pathogenesis. Biochim Biophys Acta 1809:678–685.

Locarnini S, Mason WS. 2006. Cellular and virological mechanisms of HBV drug resistance. J Hepatol 44:422–431.

Locarnini S, Zoulim F. 2010. Molecular genetics of HBV infection. Antivir Ther 15:3–14.

Lucifora J, Arzberger S, Durantel D, Belloni L, Strubin M, Levrero M, Zoulim F, Hantz O, Protzer U. 2011. Hepatitis B virus X protein is essential to initiate and maintain virus replication after infection. J Hepatol 55:996–1003.

Macovei A, Radulescu C, Lazar C, Petrescu S, Durantel D, Dwek RA, Zitzmann N, Nichita NB. 2010. Hepatitis B virus requires intact caveolin-1 function for productive infection in HepaRG cells. J Virol 84:243–253.

Macovei A, Petrareanu C, Lazar C, Florian P, Branza-Nichita N. 2013. Regulation of hepatitis B virus infection by rab5, rab7, and the endolysosomal compartment. J Virol 87:6415–6427.

McMahon BJ. 2005. Epidemiology and natural history of hepatitis B. Semin Liver Dis 25:3–8.

Meier A, Mehrle S, Weiss TS, Mier W, Urban S. 2013. Myristoylated PreS1-domain of the hepatitis B virus L-protein mediates specific binding to differentiated hepatocytes. Hepatology 58:31–42.

Nana-Sinkam SP, Croce CM. 2013. Clinical applications for microRNAs in cancer. Clin Pharmacol Ther 93:98–104.

Nassal M. 2008. Hepatitis B viruses: Reverse transcription a different way. Virus Res 134:235–249.

Neurath AR, Kent SB, Strick N, Parker K. 1986. Identification and chemical synthesis of a host cell receptor binding site on hepatitis B virus. Cell 46:429–436.

Neuveut C, Wei Y, Buendia MA. 2010. Mechanisms of HBV-related hepatocarcinogenesis. J Hepatol 52:594–604.

Noguchi C, Imamura M, Tsuge M, Hiraga N, Mori N, Miki D, Kimura T, Takahashi S, Fujimoto Y, Ochi H, Abe H, Maekawa T, Tateno C, Yoshizato K, Chayama K. 2009. G-to-A hypermutation in hepatitis B virus (HBV) and clinical course of patients with chronic HBV infection. J Infect Dis 199:1599–1607.

Ostapchuk P, Hearing P, Ganem D. 1994. A dramatic shift in the transmembrane topology of a viral envelope glycoprotein accompanies hepatitis B viral morphogenesis. EMBO J 13: 1048–1057.

Ozer A, Khaoustov VI, Mearns M, Lewis DE, Genta RM, Darlington GJ, Yoffe B. 1996. Effect of hepatocyte proliferation and cellular DNA synthesis on hepatitis B virus replication. Gastroenterology 110:1519–1528.

Patient R, Hourioux C, Sizaret PY, Trassard S, Sureau C, Roingeard P. 2007. Hepatitis B virus subviral envelope particle morphogenesis and intracellular trafficking. J Virol 81:3842–3851.

Pedersen I, David M. 2008. MicroRNAs in the immune response. Cytokine 43:391–394.

Petersen J, Dandri M, Mier W, Lutgehetmann M, Volz T, von Weizsacker F, Haberkorn U, Fischer L, Pollok JM, Erbes B, Seitz S, Urban S. 2008. Prevention of hepatitis B virus infection in vivo by entry inhibitors derived from the large envelope protein. Nat Biotechnol 26:335–341.

Pollicino T, Belloni L, Raffa G, Pediconi N, Squadrito G, Raimondo G, Levrero M. 2006. Hepatitis B virus replication is regulated by the acetylation status of hepatitis B virus cccDNA-bound H3 and H4 histones. Gastroenterology 130:823–837.

Potenza N, Papa U, Mosca N, Zerbini F, Nobile V, Russo A. 2011. Human microRNA hsa-miR-125a-5p interferes with expression of hepatitis B virus surface antigen. Nucleic Acids Res 39: 5157–5163.

Prange R, Streeck RE. 1995. Novel transmembrane topology of the hepatitis B virus envelope proteins. EMBO J 14:247–256.

Quasdorff M, Protzer U. 2010. Control of hepatitis B virus at the level of transcription. J Viral Hepat 17:527–536.

Rosler C, Kock J, Malim MH, Blum HE, von Weizsacker F. 2004. Comment on "Inhibition of hepatitis B virus replication by APOBEC3G." Science 305:1403; author reply 1403.

Rost M, Mann S, Lambert C, Doring T, Thome N, Prange R. 2006. Gamma-adaptin, a novel ubiquitin-interacting adaptor, and Nedd4 ubiquitin ligase control hepatitis B virus maturation. J Biol Chem 281:29297–29308.

Schieck A, Schulze A, Gahler C, Muller T, Haberkorn U, Alexandrov A, Urban S, Mier W. 2013. Hepatitis B virus hepatotropism is mediated by specific receptor recognition in the liver and not restricted to susceptible hosts. Hepatology 58:43–53.

Schulze A, Gripon P, Urban S. 2007. Hepatitis B virus infection initiates with a large surface protein-dependent binding to heparan sulfate proteoglycans. Hepatology 46:1759–1768.

Schulze A, Schieck A, Ni Y, Mier W, Urban S. 2010. Fine mapping of pre-S sequence requirements for hepatitis B virus large envelope protein-mediated receptor interaction. J Virol 84:1989–2000.

Schulze A, Mills K, Weiss TS, Urban S. 2012. Hepatocyte polarization is essential for the productive entry of the hepatitis B virus. Hepatology 55:373–383.

Seeger C, Mason WS. 2000. Hepatitis B virus biology. Microbiol Mol Biol Rev 64:51–68.

Somsel Rodman J, Wandinger-Ness A. 2000. Rab GTPases coordinate endocytosis. J Cell Sci 113:183–192.

Stahl M, Retzlaff M, Nassal M, Beck J. 2007. Chaperone activation of the hepadnaviral reverse transcriptase for template RNA binding is established by the Hsp70 and stimulated by the Hsp90 system. Nucleic Acids Res 35:6124–6136.

Summers J, Mason WS. 1982. Replication of the genome of a hepatitis B–like virus by reverse transcription of an RNA intermediate. Cell 29:403–415.

Tong S, Li J, Wands JR. 1995. Interaction between duck hepatitis B virus and a 170-kilodalton cellular protein is mediated through a neutralizing epitope of the pre-S region and occurs during viral infection. J Virol 69:7106–7112.

Turelli P, Mangeat B, Jost S, Vianin S, Trono D. 2004. Inhibition of hepatitis B virus replication by APOBEC3G. Science 303:1829.

Turelli P, Liagre-Quazzola A, Mangeat B, Verp S, Jost S, Trono D. 2008. APOBEC3-independent interferon-induced viral clearance in hepatitis B virus transgenic mice. J Virol 82:6585–6590.

Tuttleman JS, Pugh JC, Summers JW. 1986. In vitro experimental infection of primary duck hepatocyte cultures with duck hepatitis B virus. J Virol 58:17–25.

Urban S, Breiner KM, Fehler F, Klingmuller U, Schaller H. 1998. Avian hepatitis B virus infection is initiated by the interaction of a distinct pre-S subdomain with the cellular receptor gp180. J Virol 72:8089–8097.

van Breugel PC, Robert EI, Mueller H, Decorsiere A, Zoulim F, Hantz O, Strubin M. 2012. Hepatitis B virus X protein stimulates gene expression selectively from extrachromosomal DNA templates. Hepatology 56:2116–2124.

Vartanian JP, Henry M, Marchio A, Suspene R, Aynaud MM, Guetard D, Cervantes-Gonzalez M, Battiston C, Mazzaferro V, Pineau P, Dejean A, Wain-Hobson S. 2010. Massive APOBEC3 editing of hepatitis B viral DNA in cirrhosis. PLoS Pathog 6:e1000928.

Volz T, Allweiss L, MB MB, Warlich M, Lohse AW, Pollok JM, Alexandrov A, Urban S, Petersen J, Lutgehetmann M, Dandri M. 2013. The entry inhibitor Myrcludex-B efficiently blocks intrahepatic virus spreading in humanized mice previously infected with hepatitis B virus. J Hepatol 58:861–867.

Walter E, Keist R, Niederost B, Pult I, Blum HE. 1996. Hepatitis B virus infection of tupaia hepatocytes in vitro and in vivo. Hepatology 24:1–5.

Wang SH, Yeh SH, Lin WH, Wang HY, Chen DS, Chen PJ. 2009. Identification of androgen response elements in the enhancer I of hepatitis B virus: A mechanism for sex disparity in chronic hepatitis B. Hepatology 50:1392–1402.

Wang S, Qiu L, Yan X, Jin W, Wang Y, Chen L, Wu E, Ye X, Gao GF, Wang F, Chen Y, Duan Z, Meng S. 2012. Loss of microRNA 122 expression in patients with hepatitis B enhances hepatitis B virus replication through cyclin G(1) -modulated P53 activity. Hepatology 55:730–741.

Watanabe T, Sorensen EM, Naito A, Schott M, Kim S, Ahlquist P. 2007. Involvement of host cellular multivesicular body functions in hepatitis B virus budding. Proc Natl Acad Sci U S A 104:10205–10210.

Wei Y, Neuveut C, Tiollais P, Buendia MA. 2010. Molecular biology of the hepatitis B virus and role of the X gene. Pathol Biol (Paris) 58:267–272.

WHO. 2013. Hepatitis B (Fact sheet N°204, Updated July 2013). http://www.who.int/mediacentre/factsheets/fs204/en/

Yan H, Zhong G, Xu G, He W, Jing Z, Gao Z, Huang Y, Qi Y, Peng B, Wang H, Fu L, Song M, Chen P, Gao W, Ren B, Sun Y, Cai T, Feng X, Sui J, Li W. 2012. Sodium taurocholate cotransporting polypeptide is a functional receptor for human hepatitis B and D virus. Elife 1:e00049.

Zhang X, Zhang E, Ma Z, Pei R, Jiang M, Schlaak JF, Roggendorf M, Lu M. 2011. Modulation of hepatitis B virus replication and hepatocyte differentiation by MicroRNA-1. Hepatology 53:1476–1485.

Zoulim F, Locarnini S. 2009. Hepatitis B virus resistance to nucleos(t)ide analogues. Gastroenterology 137:1593–1608; e1591–e1592.

Zoulim F, Locarnini S. 2012. Management of treatment failure in chronic hepatitis B. J Hepatol 56:S112–S122.

Virology 454-455 (2014) 157–168

Contents lists available at ScienceDirect

Virology

journal homepage: www.elsevier.com/locate/yviro

Phagocytic cells contribute to the antibody-mediated elimination of pulmonary-infected SARS coronavirus

Fumihiko Yasui [a], Michinori Kohara [a,*], Masahiro Kitabatake [b], Tetsu Nishiwaki [c], Hideki Fujii [d,h], Chise Tateno [e], Misako Yoneda [f], Kouichi Morita [g], Kouji Matsushima [c], Shigeo Koyasu [d,i], Chieko Kai [f]

[a] Department of Microbiology and Cell Biology, Tokyo Metropolitan Institute of Medical Science, 2-1-6 Kamikitazawa, Setagaya-ku, Tokyo 156-8506, Japan
[b] Department of Immunology, Faculty of Life Sciences, Kumamoto University, 1-1-1 Honjo, Chuo-ku, Kumamoto 860-8556, Japan
[c] Department of Molecular Preventive Medicine, School of Medicine, The University of Tokyo, 7-3-1 Hongo, Bunkyo-ku, Tokyo 113-0033, Japan
[d] Department of Microbiology and Immunology, Keio University School of Medicine, 35 Shinanomachi, Shinjuku-ku, Tokyo 160-8582, Japan
[e] PhoenixBio Co., Ltd., 3-4-1 Kagamiyama, Higashihiroshima 739-0046, Japan
[f] Laboratory Animal Research Center, The Institute of Medical Science, The University of Tokyo, 4-6-1 Shirokanedai, Minato-ku, Tokyo 108-8639, Japan
[g] Department of Virology, Institute of Tropical Medicine, Nagasaki University, 1-12-4 Sakamoto, Nagasaki 852-8523, Japan
[h] Department of Immunology, Graduate School of Medicine, University of the Ryukyus, 207 Uehara, Nishihara-cho, Okinawa 903-0213, Japan
[i] Laboratory for Immune Cell System, RCAI, RIKEN Research Center for Integrative Medical Sciences (IMS-RCAI), 1-7-22 Suehiro-cho, Yokohama 230-0045, Japan

ARTICLE INFO

Article history:
Received 28 November 2013
Returned to author for revisions
10 January 2014
Accepted 4 February 2014
Available online 4 March 2014

Keywords:
SARS-CoV
B cells
CD4$^+$ T cells
Antibody
Phagocytic cells
Elimination

ABSTRACT

While the 2002–2003 outbreak of severe acute respiratory syndrome (SARS) resulted in 774 deaths, patients who were affected with mild pulmonary symptoms successfully recovered. The objective of the present work was to identify, using SARS coronavirus (SARS-CoV) mouse infection models, immune factors responsible for clearing of the virus. The elimination of pulmonary SARS-CoV infection required the activation of B cells by CD4$^+$ T cells. Furthermore, passive immunization (post-infection) with homologous (murine) anti-SARS-CoV antiserum showed greater elimination efficacy against SARS-CoV than that with heterologous (rabbit) antiserum, despite the use of equivalent titers of neutralizing antibodies. This distinction was mediated by mouse phagocytic cells (monocyte-derived infiltrating macrophages and partially alveolar macrophages, but not neutrophils), as demonstrated both by adoptive transfer from donors and by immunological depletion of selected cell types. These results indicate that the cooperation of anti-SARS-CoV antibodies and phagocytic cells plays an important role in the elimination of SARS-CoV.

Introduction

From November 2002 to July 2003, the world suffered a global outbreak of severe acute respiratory syndrome (SARS). The disease, which resulted in 8098 cases with 774 deaths, was caused by a novel type of coronavirus, termed SARS-CoV, (http://www.who.int/csr/sars/country/table2004_04_21/en/index.html). Patients with SARS usually developed a high fever followed by clinical symptoms of lower respiratory tract disease. In severe cases, the patients presented with acute respiratory distress syndrome, characterized by diffuse alveolar damage, and ultimately died (Peiris et al., 2003a, 2003b; Fowler et al., 2003; Wang and Chang 2004). The hallmarks of severe cases of SARS included high viral titer, systemic infection, lymphopenia, and over-production of proinflammatory cytokines/chemokines (often referred to as a "cytokine storm") (Wong et al., 2004; Huang et al., 2005; Cameron et al., 2007). However, there has been no subsequent consensus regarding which treatment, if any, benefited SARS patients during the outbreak (Stockman et al., 2007).

The development of an effective treatment strategy for SARS cases will require clarifying the precise mechanisms by which host immune responses control SARS-CoV infection. Cumulative evidence suggests that patients who recovered from SARS possessed specific acquired immunity based on both T and B cells (Yang et al., 2006, 2007; Li et al., 2008; Fan et al., 2009). However, the effector cells or molecules that act to eliminate SARS-CoV during the acute phase of the infection remain unclear. As the extensive outbreak of SARS has not recurred since 2003, the mechanisms by which SARS-CoV infection causes the pathogenesis and host immune responses has been investigated using adequate animal infectious models (Roberts et al., 2005, 2007; Nagata et al., 2008; Zhao et al., 2009; Zhao and Perlman, 2010). Lethal disease in BALB/c mice infected with a mouse-adapted strain of SARS-CoV, MA15, showed a lack of activation of innate immune response, resulting in a barely detectable antivirus T cell response (Zhao et al., 2009).

* Corresponding author. Tel.: +81 3 5316 3232; fax: +81 3 5316 3137.
E-mail address: kohara-mc@igakuken.or.jp (M. Kohara).

http://dx.doi.org/10.1016/j.virol.2014.02.005
0042-6822

On the other hand, aged BALB/c mice that were infected with a human clinical isolate of SARS-CoV (Urbani strain) successfully eliminated the invasive virus within 1 week post-infection; these mice exhibited high and prolonged levels of viral replication, signs consistent with clinical symptoms, and pathologic changes in the lung resembling those seen in elderly SARS patients (Roberts et al., 2005). Therefore, the infection of these aged mice is considered a model for the successful elimination of SARS-CoV by host immune responses. A recent study reported that $CD4^+$ T cells play an important role in the control of SARS-CoV infection (Chen et al., 2010). These researchers also reported an important role for innate defense mechanisms in controlling SARS-CoV infection, as demonstrated by the clearance of SARS-CoV over 9 days post-infection (dpi) in BALB/c mice depleted of both $CD4^+$ and $CD8^+$ T cells (Chen et al., 2010). These results suggest that both innate and adaptive immune responses are essential for controlling SARS-CoV infection. Nonetheless, the identity and role of effector cells and molecules participating in the elimination of SARS-CoV during the acute phase of SARS remain largely unknown.

In this study, we attempted to identify the types of immune cells that contribute to clearing SARS-CoV during the acute phase of the infection. This work employed several murine models in which hosts were deficient for (e.g., depleted via specific antibodies or lacking via immunodeficiency) or supplemented with (e.g., by adoptive transfer) individual immunologic effectors. We demonstrate that phagocytic cells (including monocyte-derived infiltrating macrophages and partially alveolar macrophages) play an important role in the elimination of SARS-CoV in mouse models of infection.

Results

Adaptive immune responses are essential for the elimination of pulmonary-infected SARS-CoV

As a first step, we confirmed the time course of viral titers in the lungs of aged (> 6 months old) BALB/c mice, young (7 weeks old) BALB/c mice, and young (8 weeks old) SCID mice following infection with SARS-CoV Vietnam/NB-04/2003. The intranasal (i.n.) infection of aged BALB/c mice with SARS-CoV resulted in over 10^8 median tissue culture infectious dose ($TCID_{50}$)/g lung tissue at 2 dpi (Fig. 1A). The infected mice exhibited histological signs of severe pneumonia, including interstitial cell thickening, immune cell infiltration, and epithelial damage in the bronchus, at 9 dpi and 21 dpi (Fig. 1B(c and d)). These results were similar to those of the previous reports that used another SARS-CoV strain such as the Urbani strain (Roberts et al., 2005). In the present work, SARS-CoV was detected in aged mice starting as early as 2 dpi (Fig. 1A). The observed titers in the aged-mouse model were considerably higher than those seen in infected young BALB/c mice, which did not show apparent histological signs of pneumonia (Fig. 2B). Titers in the aged mice remained high ($\sim 10^7$ $TCID_{50}$/g lung tissue) at 6 dpi (Fig. 1A). However, the titers decreased to levels below the lower limit of detection (LLOD; < 1000 $TCID_{50}$/g lung tissue) in the lungs of aged BALB/c mice and young BALB/c mice at 9 dpi (Fig. 1A). In contrast, young SCID mice, which lack functional T and B cells, were persistently infected with SARS-CoV during the experimental period (through 21 dpi, as shown in Fig. 1A). At this time, SCID mice did not exhibit histological signs of severe pneumonia at 9 and 21 dpi, although a high viral titer was detected in the lungs of these animals during the experimental period (Fig. 1B(g and h) and C). Recently, Zhao and Perlman (2010) obtained similar results suggesting that a mouse-adapted mutant of SARS-CoV (viral strain MA15) persistently infected RAG1 knockout mice (C57BL/6 background), animals that also lack T and B cell populations. Taken together, these results suggested that the pathogenesis of SARS does not correlate with the direct cytopathic effect of SARS-CoV. To investigate the effect of adaptive immune responses on clearance of pulmonary-infected SARS-CoV, either naïve splenocytes (obtained from BALB/c mice) or sensitized splenocytes (obtained from SARS-CoV-infected (9 dpi) BALB/c mice) were adoptively transplanted into naïve SCID mice 1 day before SARS-CoV infection. As shown in Fig. 1D, the SCID mice that received naïve splenocytes eliminated SARS-CoV from their lungs as early as the BALB/c mice did. The SCID mice transplanted with SARS-CoV-sensitized splenocytes of BALB/c mice eliminated SARS-CoV more rapidly than mice transplanted with naïve splenocytes, although the initial pulmonary viral titers were effectively the same in all groups of SCID mice at 2 dpi, with or without the transfer of splenocytes. Only one of the SCID mice that received sensitized splenocytes showed detectable lung pulmonary viral titer (3.5×10^4 $TCID_{50}$/g lung) at 6 dpi; titers in the remaining 3 animals of this group ($n=4$/time point) were below the LLOD. The SCID mice transplanted with naïve- or sensitized-splenocytes derived from aged BALB/c mice did not show histological signs of severe pneumonia at 9 dpi, although infiltration of immunocompetent cells around bronchioles (arrows) was partially observed in the lung of both groups (Fig. 1E). These results indicated that induction of adaptive immune responses is essential for the clearance of pulmonary-infected SARS-CoV.

$CD4^+$ T cells play an important role in the elimination of SARS-CoV-infected pulmonary cells, but this antiviral effect is indirect

To identify the host defense(s) involved in the elimination of SARS-CoV in the lung, we depleted $CD4^+$ cells and/or $CD8^+$ cells in BALB/c mice before and after SARS-CoV infection. Depletion of the $CD4^+$ cells or $CD8^+$ cells was performed by intravenous (i.v.) injection of (respectively) monoclonal antibody (mAb) GK1.5 or 53.6; control experiments demonstrated that injection of these mAbs produced virtually complete depletion of the corresponding cell populations (Fig. 1F). The $CD4^+$ T cell-depleted BALB/c mice and the $CD4^+$ T and $CD8^+$ T cell-double-depleted BALB/c mice failed to eliminate the SARS-CoV-infected pulmonary cells by 9 dpi (Fig. 1G). In contrast, the $CD8^+$ T cell-depleted BALB/c mice largely eliminated the SARS-CoV-infected pulmonary cells by 9 dpi (Fig. 1G). Recently, Chen et al. (2010) reported that both $CD4^+$ T cells and neutralizing antibodies (following antibody response) play an important role in the elimination of SARS-CoV-infected pulmonary cells. However, it remains unclear whether the elimination of the virus in the present work and by Chen et al. (2010) reflects direct antiviral effect(s) by $CD4^+$ T cells and/or B cells. Notably, several reports have demonstrated the presence of $CD4^+$ T cells with cytotoxic activity during persistent viral infection, including infection by human immunodeficiency virus, human cytomegalovirus, and Epstein–Barr virus (Appay et al., 2002; Casazza et al., 2006; Landais et al., 2004). Furthermore, $CD4^+$ T cell-mediated control of a γ-herpes virus in B cell-deficient mice is mediated by interferon-gamma (IFN-γ) (Christensen et al., 1999). In the present work, we found that SARS-CoV persistently infected the lung of nude (T cell-deficient) mice, as well as SCID mice (deficient of T cell and B cell), without inducing histological signs of pneumonia (Fig. 2A and B). Therefore, we investigated (using either of two models) whether $CD4^+$ T cells could directly eliminate SARS-CoV via IFN-γ secretion. Our first model consisted of the adoptive transfer, 1 day before SARS-CoV infection, of $CD4^+$ cells (1×10^7 cells/mouse) from BALB/c mice into nude mice and SCID mice. The SCID mice that received the $CD4^+$ T cell transfer did not eradicate SARS-CoV infection by 9 dpi (Fig. 2C). In contrast, nude mice that received the same quantity of $CD4^+$ cells decreased the pulmonary viral titer below

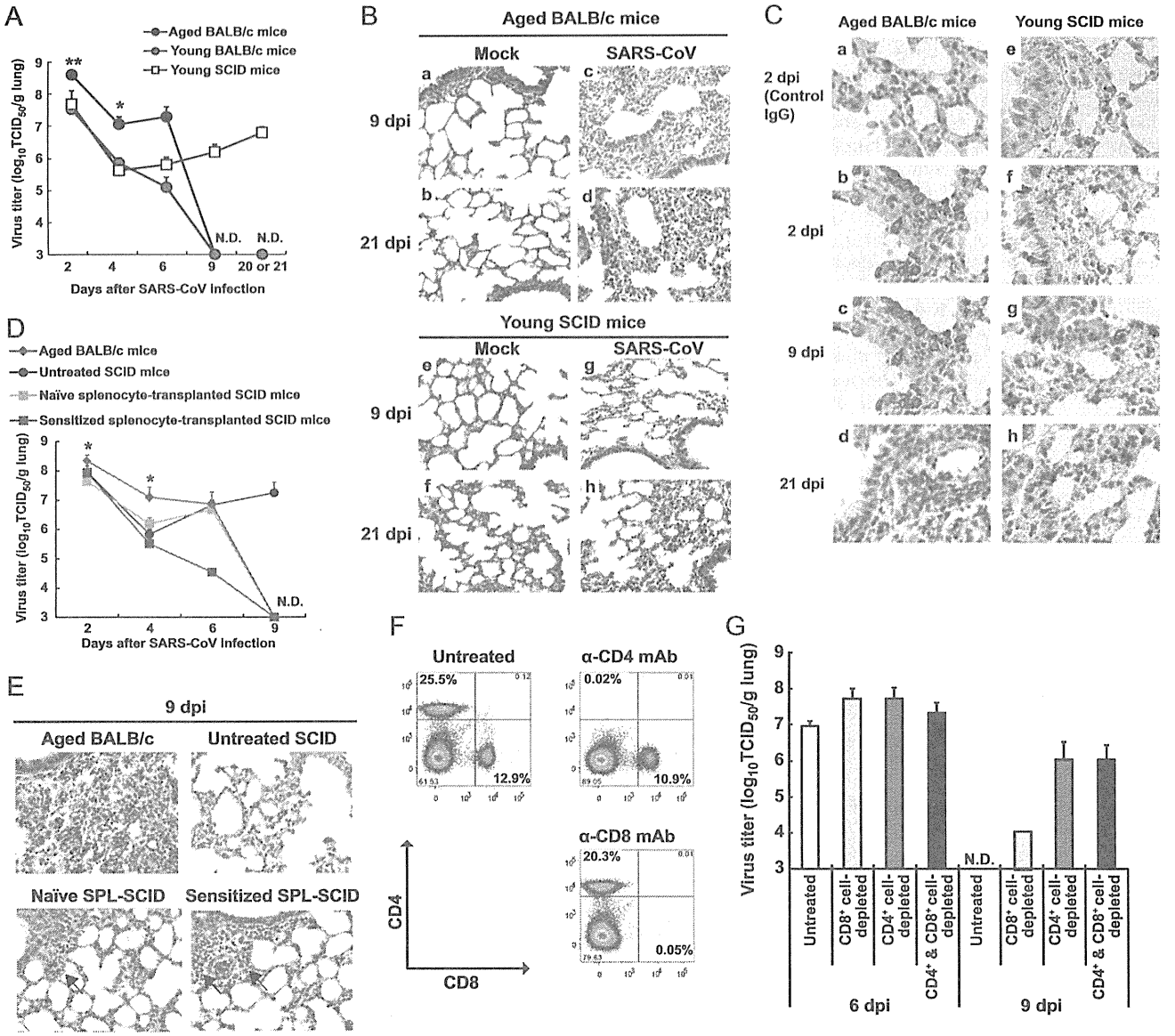

Fig. 1. $CD4^+$ T cells play an important role in the control of SARS-CoV infection. (A–C) aged BALB/c mice (n=4–7/time point), young BALB/c mice (n=5–10/time point), and young SCID mice (n=4–8/time point) were infected intranasally with 1×10^5 $TCID_{50}$ of SARS-CoV Vietnam strain. (A) Virus titers in the lung ($TCID_{50}$/g lung tissue) of aged BALB/c mice (closed circles), young BALB/c mice (gray circles), or young SCID mice (open squares) sacrificed at 2, 4, 6, 9, or 21 dpi (except for 20 dpi in young BALB/c mice). $^*p < 0.05$, $^{**}p < 0.01$ (compared with young BALB/c mice and SCID mice at the respective time point). N.D.: not detected. (B) Representative lung sections (hematoxylin and eosin staining; section thickness 4 μm) from aged BALB/c mice at 9 dpi (a and c) and 21 dpi (b and d) and from young SCID mice at 9 dpi (e and g) and 21 dpi (f and h). For all micrographs, original magnification is 200 ×. (C) Detection of virus-infected cells in the lungs at 2, 9, or 21 dpi (SARS-CoV nucleocapsid protein [brown staining]; original magnification, 400 ×). (D) Temporal change of pulmonary virus titer in the following: aged BALB/c mice (green); untreated SCID mice (blue); SCID mice transplanted with splenocytes from naïve BALB/c mice (yellow); or SCID mice transplanted with splenocytes from sensitized BALB/c mice (red). Splenocytes (4×10^7 cells) were administered intravenously to each recipient SCID mouse 1 day before infection. Data are presented as mean ± S.D. (n=4/time point). $^*p < 0.05$ (compared with naïve splenocyte-transplanted SCID mice at 2 dpi or with other groups at 4 dpi). (E) Representative lung sections (hematoxylin and eosin staining; section thickness 4 μm) from each group in (D) at 9 dpi. SPL, splenocyte. For all micrographs, original magnification is 200 ×. (F) Flow cytometry analysis of CD4 and CD8 expression on lymphocytes isolated from spleen 1 day after administration of the indicated mAb. (G) Virus titers in the lung of untreated (white), $CD8^+$ cell-depleted (light gray), $CD4^+$ cell-depleted (dark gray), or $CD4^+$ and $CD8^+$ cell-depleted BALB/c mice (black) at 6 and 9 dpi. The limit of detection was $< 1 \times 10^3$ $TCID_{50}$/g lung. Data are presented as mean ± S.D. (n=3–7/time point).

the LLOD between 6 and 9 dpi (Fig. 2D). For our second model, we investigated the effect of IFN-γ on the elimination of SARS-CoV by using IFN-γ-deficient mouse models. The IFN-γ-deficient mice and the SCID mice that received splenocytes from IFN-γ deficient mice controlled the SARS-CoV infection as well as the wild-type mice did (Fig. 2E). These results demonstrated that $CD4^+$ T cells are an essential cell type for the control of SARS-CoV infection, and that the effect of this cell fraction is indirect.

B cells and anti-SARS-CoV antibodies contribute to the control of SARS-CoV infection

The above results showed that SARS-CoV infection could be controlled both by nude mice which received $CD4^+$ cells and by $CD8^+$ cell-depleted BALB/c mice, suggesting that B cell is implicated in the elimination of SARS-CoV. So far, there are multiple studies that demonstrated the prophylactic effect of neutralizing antibodies against

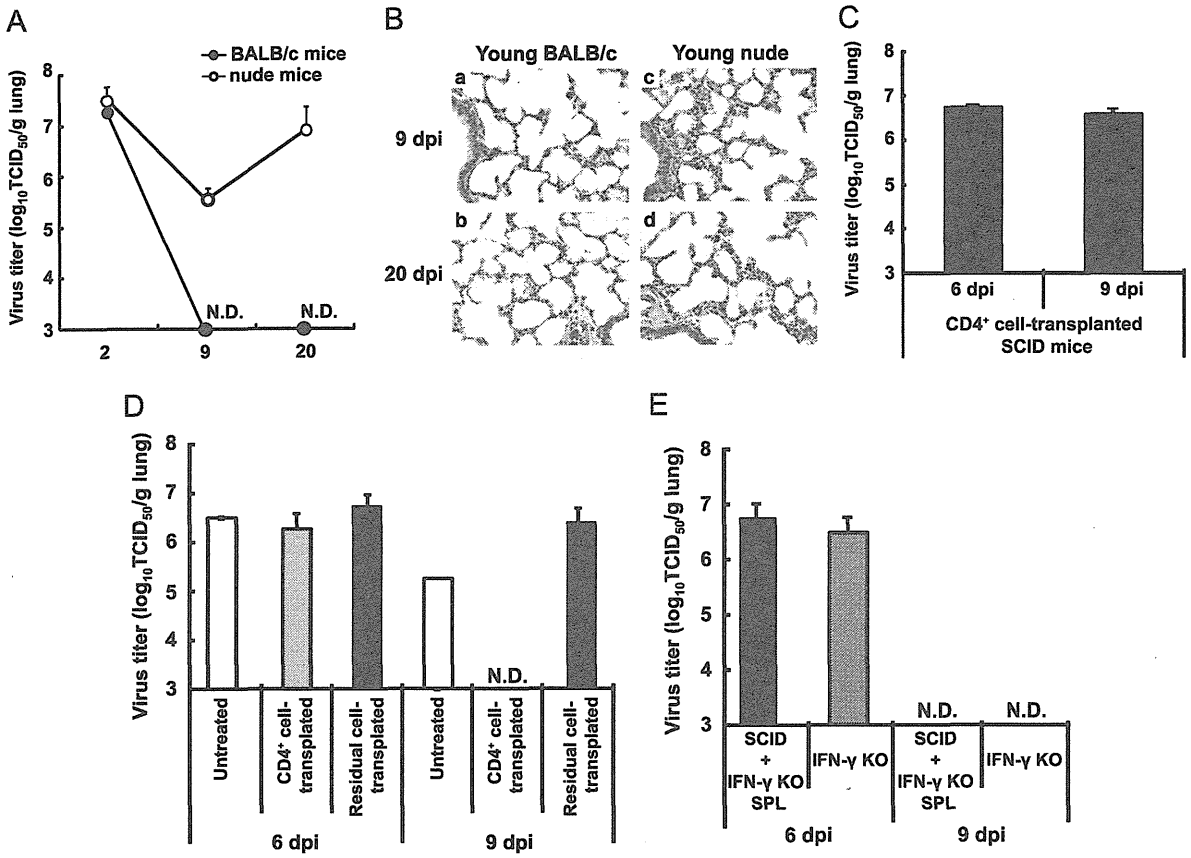

Fig. 2. Antiviral effect of $CD4^+$ cells is indirect. (A) Temporal change of virus titer in the lung of young BALB/c mice (closed circles) and young nude mice (open circles). Data are presented as mean ± S.D. (n=5/time point). N.D.: not detected. (B) Representative lung sections (hematoxylin and eosin staining; section thickness 4 μm) from young BALB/c mice at 9 dpi (a) and 20 dpi (b) and young nude mice at 9 dpi (c) and 20 dpi (d). For all micrographs, original magnification is 200 ×. (C) Virus titer in the lung of $CD4^+$ cell-transplanted SCID mice was determined at 6 and 9 dpi. Data are presented as mean ± S.D. (n=5/time point). $CD4^+$ cells (1×10^7 cells) were administered to each recipient SCID mouse intravenously 1 day before challenge. (D) Virus titer in the lung of nude mice adoptively transplanted with $CD4^+$ cells (gray) or residual cells ($CD4^-$ cells; black), determined at 6 and 9 dpi. Untreated nude mice (white) were included as a control. $CD4^+$ cells (1×10^7 cells) or residual cells (3×10^7 cells) were administered to each recipient nude mouse intravenously 1 day before challenge. Data are presented as mean ± S.D. (n=3/time point). (E) Pulmonary virus titer of IFN-γ deficient mice and splenocyte-transplanted SCID mice at 6 and 9 dpi. Splenocytes (4×10^7 cells) derived from IFN-γ deficient mice were administered to each recipient SCID mouse intravenously 1 day before challenge. Data are presented as mean ± S.D. (n=3/time point). N.D.: not detected. SPL, splenocyte.

SARS-CoV in animal models. (Casazza et al., 2006; Landais et al., 2004; Christensen et al., 1999; Nicholls et al., 2003; Lee et al., 2003; Peiris et al., 2004). Furthermore, we examined whether B cells play an important role in the elimination of SARS-CoV in the lung by using SCID mice that were transplanted with B cells of naïve BALB/c mice before infection with the virus. Although the $CD19^+$ cell-transplanted SCID mice ($CD19^+$ cells; purity 98.3%) did not decrease the pulmonary SARS-CoV titer by 9 dpi, the SCID mice that had received a combination of both cell fractions (the $CD19^+$ cell subset and the residual cell subsets ($CD19^-$ subsets containing T cells)) exhibited marked decreases in pulmonary SARS-CoV titer (to less than 1×10^4 $TCID_{50}$/g lung tissue; Fig. 3A). SCID mice that received the residual cell subsets alone (i.e., a $CD19^-$ fraction) also did not exhibit decreased pulmonary SARS-CoV titer by 9 dpi (Fig. 3A).

To examine whether post-infection treatment with anti-SARS-CoV Abs could control SARS-CoV infection, SCID mice were infected i. n. with SARS-CoV and then were administered intraperitoneally (i.p.) twice with 0.5 mL of rabbit anti-spike (S) protein antiserum (neutralization titer [NT_{50}] > 300 against SARS-CoV; raised against SARS-CoV S protein expressed via recombinant vaccinia virus (Kitabatake et al., 2007; Yasui et al., 2008)). The group treated with anti-S protein antiserum eliminated SARS-CoV infection, but neither control group (treated with normal rabbit serum or rabbit antiserum raised against non-recombinant vaccinia virus) eliminated SARS-CoV infection (Fig. 3B). The decrease of pulmonary-infected SARS-CoV titer in the anti-S protein antiserum-treated SCID mice was confirmed by quantitative RT-PCR for the detection of mRNA of the nucleocapsid (N) protein-encoding gene of SARS-CoV (Fig. 3C). These results suggested that the production of anti-SARS-CoV Abs by B cells, which is a T cell-dependent process, plays an important role in the control of SARS-CoV infection.

Neutralizing activity of antisera against SARS-CoV is not essential for the control of SARS-CoV infection

Multiple studies have demonstrated that neutralizing Abs are important humoral factors for the control of viral infection. As shown in Fig. 3B, administration of high-dose neutralizing Abs (NT_{50} > 300; 0.5 mL × 2 doses) eliminated SARS-CoV, although the antisera used were derived from other animal species. However, when BALB/c mice eradicated the SARS-CoV infection (9 dpi), the neutralization titer of antiserum from these BALB/c mice achieved an NT_{50} of 40–80 (Yasui et al., 2008). To investigate whether the neutralizing activity of Abs is crucial for controlling SARS-CoV infection, the SARS-CoV-infected SCID mice were administered i.p. at 6 dpi with lower doses of either mouse anti-SARS-CoV antiserum or rabbit anti-S protein antiserum. For this experiment, the neutralization titers of both mouse anti-SARS-CoV antiserum and rabbit

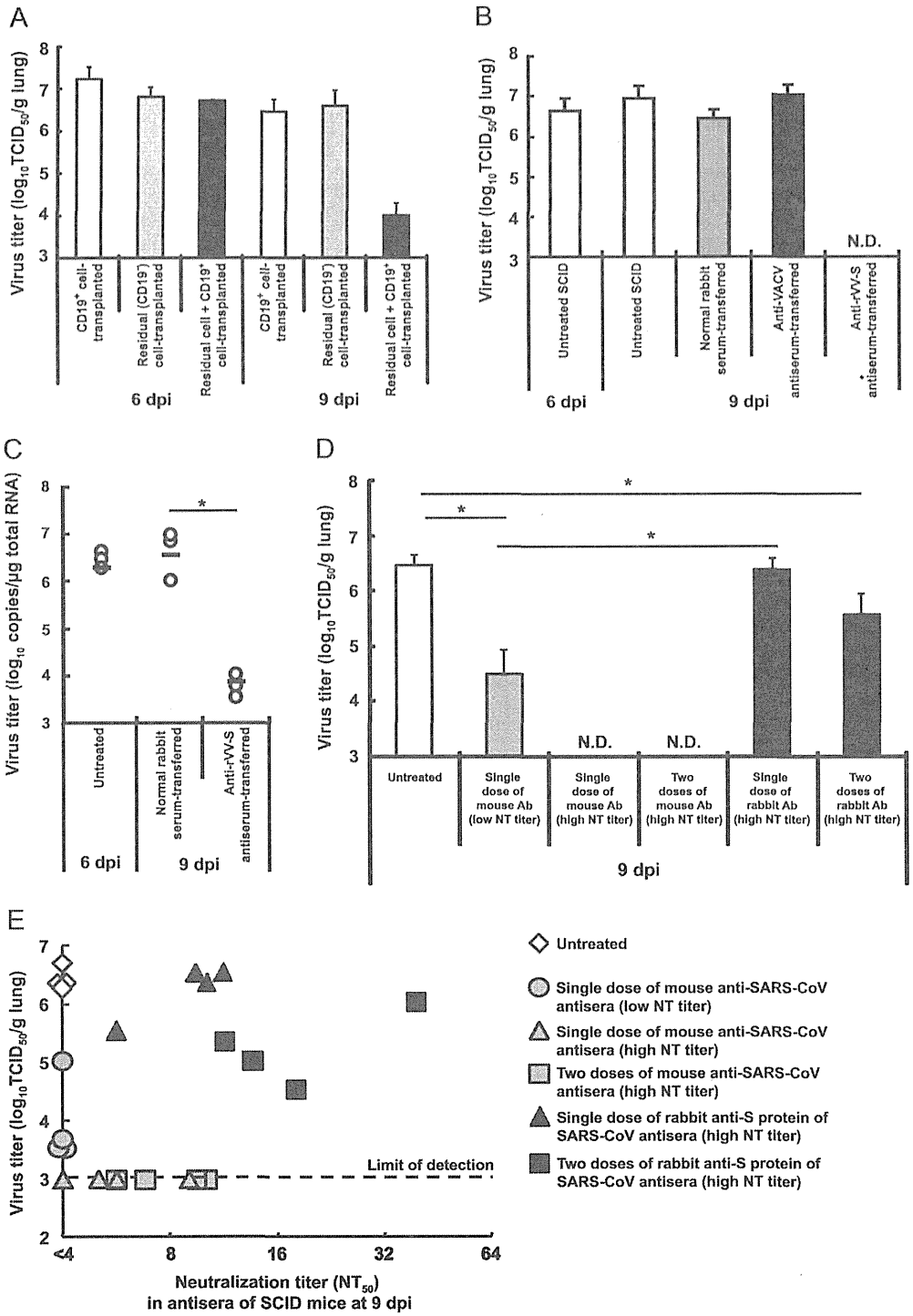

Fig. 3. Clearance of SARS-CoV with anti-SARS-CoV antibodies does not correlate with neutralizing activity. (A) Virus titers in the lung of SCID mice adoptively transplanted with $CD19^+$ cells (white), residual cells ($CD19^-$ cells; gray), or both $CD19^+$ and $CD19^-$ cells (black) were determined at 6 and 9 dpi. $CD19^+$ cells (2×10^7 cells) and/or residual cells (2×10^7 cells) were administered to each recipient SCID mouse intravenously 1 day before challenge. Data are presented as mean ± S.D. (n=3–4 mice/time point). (B) Antiviral effect of post-infection administration of rabbit anti-S (spike) protein of SARS-CoV antibody ($NT_{50} > 300$) (at 6 and 8 dpi) assessed as pulmonary virus titer at 9 dpi; untreated (white), normal rabbit serum-injected (gray), anti-vaccinia virus (VACV) antiserum (black), or anti-recombinant vaccinia virus expressing S protein of SARS-CoV (rVV-S) antiserum-injected (anti-S protein of SARS-CoV antiserum-injected). Data are presented as mean ± S.D. (n=5 mice/time point). N.D.: not detected. (C) Quantitation of mRNA of nucleocapsid protein-encoding gene of SARS-CoV in the lung of SCID mice administered with anti-S protein antiserum. Total RNA extracted from the lungs was used to measure mRNA of nucleocapsid protein-encoding gene of SARS-CoV by quantitative RT-PCR. Each symbol indicates an individual subject. Heavy horizontal bars indicate the mean values for each treatment. *$p < 0.05$. (D) Antiviral effect of post-infection treatment with murine anti-SARS-CoV antiserum or rabbit anti-S (spike) protein of SARS-CoV antiserum at low neutralization titer in SCID mice infected with SARS-CoV. A single dose of antiserum (0.2 mL) was injected at 6 dpi at low (NT_{50}=13.3) or high (NT_{50}=40) neutralization titer. Two doses of antiserum (0.2 mL/dose) were injected at 6 and 8 dpi at high (NT_{50}=40) neutralization titer. The limit of detection was $< 1 \times 10^3$ $TCID_{50}$/g lung. Data are presented as mean ± S.D. (n=4 mice/group). *$p < 0.05$. N.D.: not detected. (E) Relationship between pulmonary virus titer and neutralization titer against SARS-CoV in sera of SCID mice adoptively transplanted with murine anti-SARS-CoV antiserum or rabbit anti-S protein of SARS-CoV antiserum at 9 dpi; untreated group (open diamond), single dose of low-dose (NT_{50}=13.3, 0.2 mL; 6 dpi) murine anti-SARS-CoV antiserum (gray circle), single dose of high-dose (NT_{50}=40, 0.2 mL) murine anti-SARS-CoV antiserum (gray triangle), two doses of high-dose (NT_{50}=40, 0.2 mL × 2; 6 and 8 dpi) murine anti-SARS-CoV antiserum (gray square), single dose of high-dose rabbit anti-S protein antiserum (closed triangle), two doses of high-dose rabbit anti-S protein antiserum (closed square). Note that symbol colors match classifications in panel (D).

anti-S protein antiserum were adjusted to $NT_{50}=40$; mouse anti-SARS-CoV antiserum also was tested at $NT_{50}=13.3$. As shown in Fig. 3D, the single injection (0.2 mL i.v., $NT_{50}=40$) of mouse SARS-CoV antiserum, but not that of rabbit anti-S protein antiserum, reduced the pulmonary SARS-CoV titer. The single injection of mouse anti-SARS-CoV antiserum at an even lower neutralization titer (0.2 mL, $NT_{50}=13.3$) also reduced the pulmonary virus titer by greater than 100-fold compared with that of untreated animals. Importantly, the SCID mice treated with rabbit anti-S protein antiserum did not eliminate SARS-CoV by 9 dpi, although the antisera of SCID mice treated with the rabbit antiserum clearly demonstrated neutralization activity against SARS-CoV (Fig. 3E). The inconsistency between the in vitro (neutralizing activity) and in vivo (clearance of pulmonary SARS-CoV) activities of the rabbit antiserum suggested that other effectors, besides anti-SARS-CoV Abs, also might be required to control SARS-CoV infection.

Phagocytic cells are essential for the elimination of the SARS-CoV-infected pulmonary cells in the presence of anti-SARS-CoV antibodies

To identify the effectors involved in the elimination of SARS-CoV-infected pulmonary cells in our mouse models, we tested the contribution of several candidate effectors. SARS-CoV-infected BALB/c mice were depleted of the first candidate, complement, by the injection of cobra venom factor (CVF; 40 U/mouse) at 5 and 6 dpi. Despite the depletion of C3 from the serum of BALB/c mice following CVF injection (Fig. 4A), CVF-treated BALB/c mice still eliminated SARS-CoV by 9 dpi (Fig. 4B). These results demonstrated that the complement–antibody complex is not required for the control of SARS-CoV infection in this model.

We next investigated the contribution of NK cells to the elimination of SARS-CoV by administering anti-IL-2Rβ mAb (TM-β1), a treatment known to result in long-term depletion of NK cells (Tanaka et al., 1993). We injected i.p. TM-β1 (100 μL of ascites) into both SCID and BALB/c mice. Three days after TM-β1 treatment, NK cell-depleted BALB/c mice splenocytes were transferred adoptively into NK cell-depleted SCID mice. The SCID mice were infected i.n. with SARS-CoV at 1 day after the splenocyte transfer. As shown in Fig. 4C, NK cells were considerably depleted in both the donor BALB/c mice (spleen) and the recipient SCID mice. However, virus still was eradicated in this NK-depleted model (Fig. 4D); thus, Ab-dependent cell-mediated cytotoxicity, which requires NK cells, was excluded as a mechanism for the elimination of SARS-CoV.

Other blood cells also may serve as effectors for the control of SARS-CoV. Specifically, elevated levels of alveolar macrophages, monocyte-derived infiltrating macrophages, and neutrophils were observed in many SARS patients (Nicholls et al., 2003; Lee et al., 2003). While these three cell types have been implicated in SARS pathology, the role of these cell subsets in the control of SARS-CoV infection is still unknown. To investigate the role of these myeloid cells in the clearance of SARS-CoV-infected pulmonary tissue, each subset of these myeloid cells was depleted by administration of a specific mAb or reagent. Consistent with previous reports (Pribul et al., 2008), alveolar macrophages were depleted for more than 5 days following i.n. administration of 100 μL of 30% clodronate liposome (Fig. 5A). (Note that we used 30% clodronate liposome, thereby avoiding the intensive infiltration of neutrophils seen with administration of 100% clodronate liposome (Fig. 5A)). Neutrophils ($CD11b^+$ and $Ly\text{-}6G^{hi}$) and $Gr\text{-}1^{int}$ monocytes in blood and lung were significantly depleted for at least 3 days after i.p. treatment with 250 μg of anti-Gr-1 mAb, whereas neutrophils alone were depleted upon administration of anti-Ly-6G mAb (1A8) (Fig. 5B and Daley et al., 2008). The $Gr\text{-}1^+$ cell- and/or alveolar macrophage-depleted groups failed to eliminate the pulmonary SARS-CoV infection (Fig. 5C), whereas the alveolar macrophage-depleted group showed partial elimination of the virus. In contrast, the neutrophil-depleted BALB/c animals (anti-Ly-6G mAb-treated mice) eliminated SARS-CoV by 9 dpi (Fig. 5C). Importantly, the neutralizing Ab titer of these cell-depleted mice was comparable to that of untreated BALB/c mice (Fig. 5D, $p=0.37$). Similar results were obtained in murine anti-SARS-CoV antisera-treated SCID mice that were administered with clodronate liposome and/or anti-Gr-1 mAb (Fig. 5E). These results suggest that phagocytic cells, especially monocyte-derived infiltrating macrophages, cooperate with anti-SARS-CoV Abs to provide control of SARS-CoV infection in these mouse models.

Discussion

The outbreak of SARS in 2002–2003 resulted in over 8000 cases, with 10% mortality. The worst symptoms might correlate with age-dependent defects of immune response, given that mortality exceeded 50% in patients over 65 years of age (Peiris et al., 2004). A recent study using MA15-infected mouse models suggested that age-dependent increases of prostaglandin D2 expression in the lung may be associated with impaired immune response (Zhao et al., 2011). Retrospective analyses of recovered SARS patients suggests that patients who recovered from SARS possessed specific acquired immunity based on both T and B cells (Yang et al., 2006, 2007; Li et al., 2008; Fan et al., 2009). Notably, most patients who recover from SARS had elevated and sustained levels of neutralizing Abs, and patients with longer illnesses exhibited lower levels of neutralizing Abs than did patients with shorter durations of illness (Temperton et al., 2005; Ho et al., 2005). Previous studies revealed that passive transfer of immune serum to naïve animals prevented SARS-CoV replication in the lower respiratory tract (Yang et al., 2004; Subbarao et al., 2004; Kam et al., 2007; Zhu et al., 2007; Rockx et al., 2008, 2011). Taken together, these results suggest that Ab responses likely play an important role in determining the ultimate disease outcome of SARS-CoV infection. Virus could be eradicated by direct binding of the virus by the neutralizing Abs and/or by cooperation between virus-specific Abs and other effector cells, including complement, NK cells, and phagocytic cells. However, the actual mechanism that controls the acute phase of SARS-CoV infection remained unclear.

In this study, we found that rabbit antiserum raised against the S protein of SARS-CoV exhibited significantly lower efficacy in the control of the virus infection than mouse anti-SARS-CoV antiserum when similar neutralization titers against SARS-CoV were transferred into recipient mice. Therefore, it appears that the neutralization activity of Ab against SARS-CoV does not correlate with the clearance efficacy of the virus from infected murine lung. On the other hand, some other antibody property (such as avidity) may differ between the murine and rabbit antisera, given that the former is a polyclonal species derived from SARS-CoV-infected mice, while the latter was generated in rabbit against the S protein. Further study will be needed to resolve this distinction. In a Chinese hamster model of SARS, post-infection treatment (at 1 dpi) with 100 mg/kg of equine neutralizing $F(ab')_2$ resulted in only partial reduction of pulmonary viral titer, although prophylactic treatment at a 10-fold lower dose was sufficient to completely block SARS-CoV infection (Luo et al., 2007). This result suggests that the anti-infective activity of a neutralizing Ab is mediated primarily via prevention of SARS-CoV invasion; the neutralizing Ab plays a lesser role in eliminating the virus after establishment of infection.

Therefore, we focused on the cooperation between anti-SARS-CoV Abs and other effectors in the control of SARS-CoV infection. Candidate effectors include complement (e.g., C3 and other

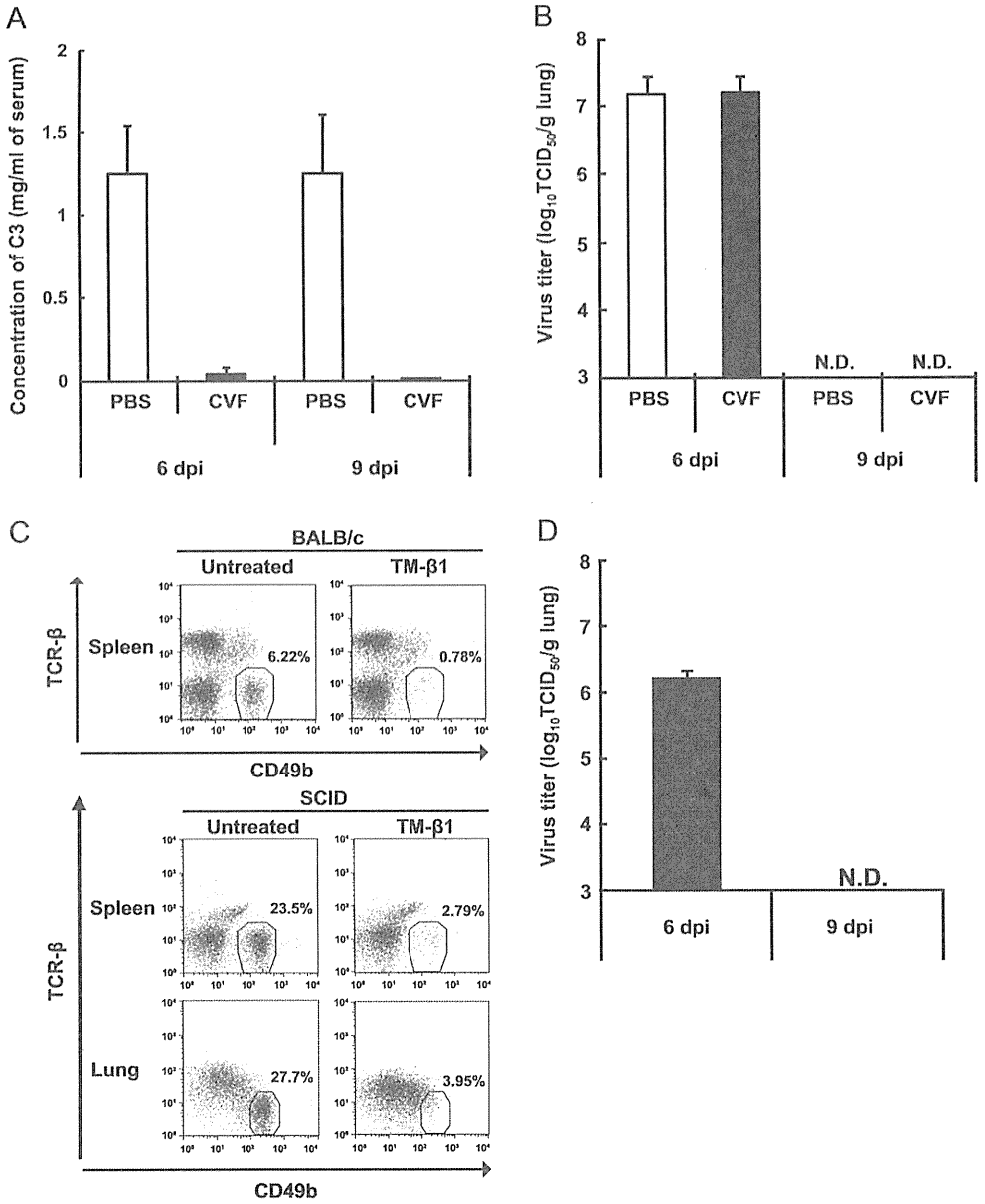

Fig. 4. Complement and NK cells are not required for the control of pulmonary-infected SARS-CoV. For panels (A) and (B), complement was depleted in BALB/c mice by administering cobra venom factor (CVF) intravenously at 5 dpi and 6 dpi; control animals were administered phosphate-buffered saline (PBS) by the same regimen. (A) Concentration of complement 3 in the sera of BALB/c mice was measured by ELISA. Data are presented as mean ± S.D. (n=4/time point). (B) Pulmonary virus titer of aged BALB/c mice treated with CVF (complement depletion), determined at 6 and 9 dpi. Data are presented as mean ± S.D. (n=4/group). N.D.: not detected. For panels (C) and (D), NK cells were depleted by administering anti-IL-2Rβ Ab (TM-β1). Untreated BALB/c mice were used as controls. (C) Flow cytometric analysis of CD49b and TCRβ expression of leukocytes in the spleen of BALB/c mice 3 days after the administration of TM-β1 and in spleen and lung of SCID mice 4 days after the administration of TM-β1. Representative diagrams are shown. (D) Splenocytes from BALB/c mice administered with TM-β1 were adoptively transplanted into SCID mice that were previously administered with TM-β1 to deplete NK cells. Pulmonary virus titers of BALB/c splenocyte-transplanted SCID mice were determined at 6 and 9 dpi. Data are presented as mean ± S.D. (n=3–4/group). N.D.: not detected.

members of the complement–antibody complex pathway), NK cells (mediators of the Ab-dependent cell-mediated cytotoxicity pathway), and Fc gamma receptor (FcγR)-bearing cells (notably alveolar macrophages, monocytes [monocytes-derived infiltrating macrophages], and neutrophils). A previous study reported that anti-Gr-1 mAb (RB6-8C5) recognizes not only neutrophils but also additional leukocyte populations, including monocytes (Daley et al., 2008). Therefore, we used both anti-Gr-1 mAb and neutrophil-specific mAb (anti-Ly-6G mAb) to discriminate monocytes and neutrophils. We tested the role of these candidates by selective depletion of a mouse infection model for various factors using CVF (complement depletion), anti-IL-2Rβ mAb (TM-β1; NK cell depletion), clodronate liposomes (alveolar macrophage depletion), anti-Gr-1 mAb (monocytes/neutrophil depletion), or anti-Ly6G mAb (neutrophil depletion) before or after SARS-CoV infection. Notably, the groups administered with clodronate liposome or anti-Gr-1 mAb, but not those treated with anti-Ly-6G mAb, failed to eliminate SARS-CoV from their lungs by 9 dpi. Our results indicated that phagocytic cells such as monocyte-derived infiltrating macrophages and partially alveolar macrophages, but not neutrophils, play a crucial role in the elimination of SARS-CoV-infected pulmonary cells in mice. Although little is known about

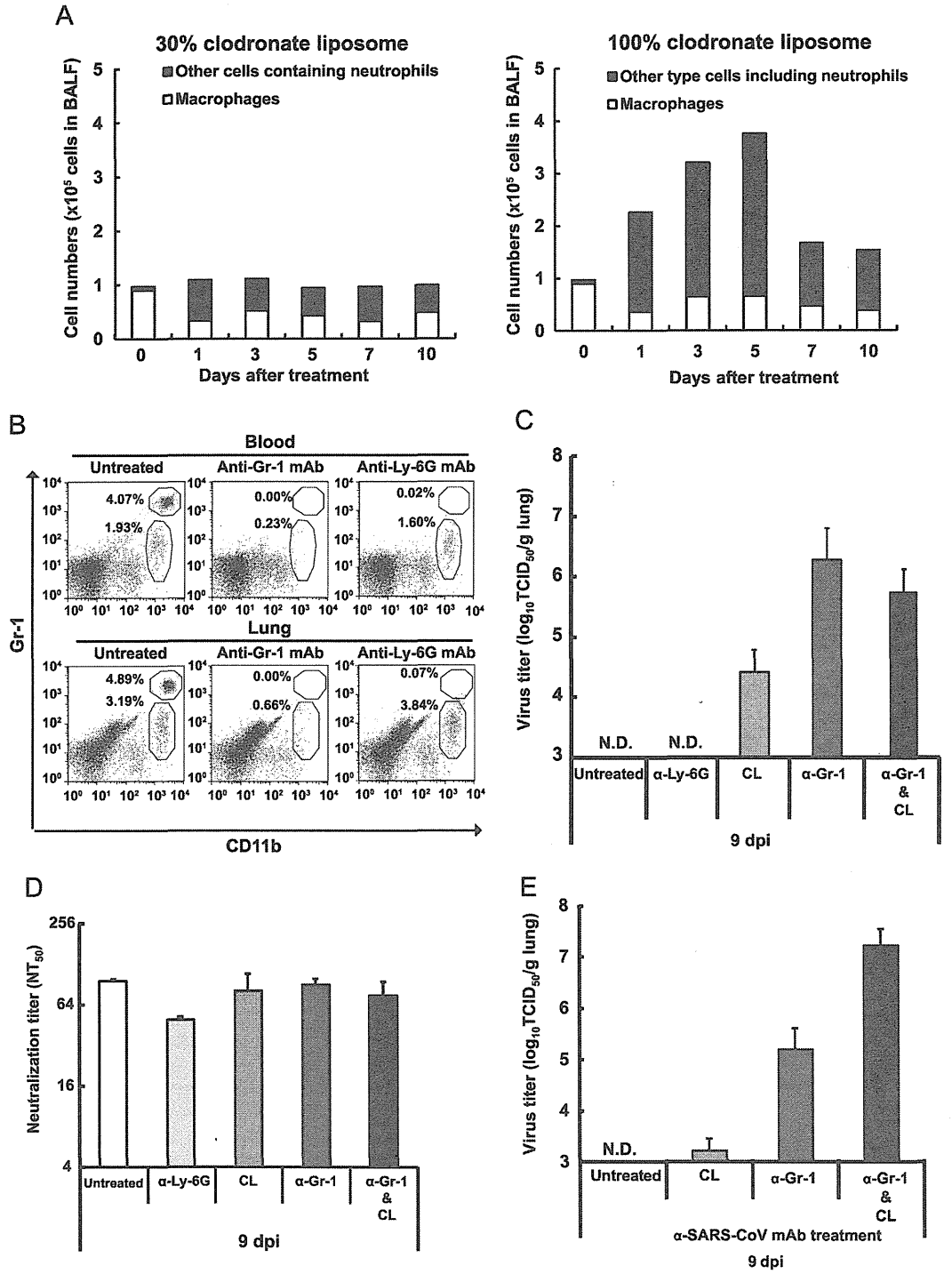

Fig. 5. Cooperation of phagocytic cells and antibodies is essential for the eradication of SARS-CoV infection. (A) Depletion of alveolar macrophages by intranasal administration of clodronate liposome. BALB/c mice were administered intranasally with 0.1 mL of 30% (left graph) or 100% clodronate liposome (right graph). Where applicable, dilution of clodronate liposome (to 30%) was performed using Dulbecco's PBS. Numbers of cells in bronchoalveolar lavage fluid (BALF) were determined by counting cell numbers (white, alveolar macrophages; black, other cells including neutrophils) following cytospin preparation. Data are presented as mean (n=2/time point). (B) Depletion of neutrophils and monocytes with anti-Gr-1 monoclonal antibody (mAb) or anti-Ly-6G mAb (respectively). The panel shows results of flow cytometric analysis of CD11b and Gr-1 expression of leukocytes in blood and lung of BALB/c mice at 3 days after the administration of anti-Gr-1 mAb or anti-Ly-6G mAb. Untreated BALB/c was used as a control. Representative diagrams are shown. (C) Pulmonary virus titers of BALB/c mice that were administered anti-Ly-6G mAb (depletion of neutrophils), clodronate liposome (depletion of alveolar macrophages; gray), anti-Gr-1 mAb (depletion of Gr-1$^+$ cells; dark gray), or both clodronate liposome and anti-Gr-1 mAb (black) were determined 9 dpi. Data are presented as mean ± S.D. (n=3–7/group). N.D.: not detected. CL: clodronate liposome. (D) Neutralization titers against SARS-CoV in antisera of SARS-CoV-infected mice at 9 dpi. (E) Pulmonary virus titers of passively immunized SCID mice (i.e., injected with anti-SARS-CoV antiserum) that were administered clodronate liposome (CL; depletion of alveolar macrophages; gray), anti-Gr-1 mAb (depletion of Gr-1$^+$ cells; dark gray), or both CL and anti-Gr-1 mAb (black) were determined at 9 dpi. Data are presented as mean ± S.D. (n=3–6/group). N.D.: not detected.

host defense mechanisms in the acute phase of SARS clinical infection, infiltration of large numbers of macrophages into the lungs of SARS patients was observed (Nicholls et al., 2003; Franks et al., 2003). Those reports are consistent with our results, although further studies are necessary to clarify the mechanism (s) of elimination of SARS-CoV via cooperation of phagocytic cells and SARS-CoV-specific antibodies.

While a previous study (Chen et al., 2010) and our results (Fig. 1G) showed that depletion of $CD8^+$ T cell at the time of infection had little effect on viral replication or clearance, Zhao and Perlman (2010) reported that adaptive transfer of $CD8^+$ T cells sensitized with the SARS-CoV MA 15 strain into naïve BALB/c mice completely protected the recipients from a subsequent challenge with lethal dose of MA15. Zhao et al. also showed that the diminished virus-specific $CD8^+$ T cell responses resulted from inefficient activation of alveolar macrophages and respiratory dendritic cells in lethal diseases (Zhao et al., 2009, 2012; Zhao and Perlman, 2010). Their studies also demonstrated suboptimal responses of $CD4^+$ T cell responses as well as $CD8^+$ T cells, implying a critical role for antibody responsiveness in the MA15 infection model. In addition, while depletion of alveolar macrophages before MA15 infection completely protected mice from this lethal challenge, the depletion of alveolar macrophages at 2 days after MA15 infection appeared to exacerbate mortality (Zhao et al., 2009). Therefore, our findings would be rendered more persuasive by the inclusion of additional animal infection experiments using other patient isolates, such as the Urbani strain, and mouse-adapted strains, such as MA15, of SARS-CoV.

Although the importance of other effector cells for clearance of coronaviruses is still unknown, there are several reports that showed the implication of FcγR-bearing cells in the clearance of influenza virus. Fujisawa (2008) noted that neutrophils play a crucial role in the control of influenza virus infection by cooperation with anti-influenza virus antibodies. It also has been reported that $FcR\gamma^{-/-}$ mice were highly susceptible to influenza virus infection, even in the presence of anti-influenza Abs from immune $FcR\gamma^{+/+}$ mice (Huber et al., 2001). These results indicate the important role of FcγR-bearing effector cells in the clearance of influenza virus infections. In addition, we here demonstrated that both monocyte-derived macrophages (infiltrating-type) and partially alveolar macrophages (resident-type) contribute to the elimination of SARS-CoV-infected pulmonary cells in the presence of anti-SARS-CoV Abs.

Alveolar macrophages play a central role in maintaining lung homeostasis and are considered the first line of host defense against respiratory microbes. Marked enhancement of the virus titer was reported in other respiratory virus infection models (Pribul et al., 2008; Tumpey et al., 2005). On the other hand, monocytes circulate throughout the body in anticipation of inflammation and infection. Murine monocytes are reported to comprise two distinct subpopulations with different phenotypes: $CX3CR1^{lo}CCR2^+Gr\text{-}1^+$ and $CX3CR1^{hi}CCR2^-Gr\text{-}1^-$ monocytes (Geissmann et al., 2003). On infiltration of the infection site, $Gr\text{-}1^+$ inflammatory monocytes can give rise to various dendritic cells and macrophage types (Varol et al., 2009). Iijima et al. (2011) demonstrated that $Gr\text{-}1^+$ monocyte-derived APCs are required to elicit IFN-γ secretion from effector Th1 cells, thus mediating host protection against HSV-2 infection. Lin et al. (2008) reported that monocyte-derived DCs and macrophages cause immune pathology rather than viral clearance during influenza virus infection. In contrast, $Gr\text{-}1^+$ monocyte-derived cells are involved in the clearance of SARS-CoV infection, although the role of $Gr\text{-}1^+$ monocyte-derived cells in the development of pathogenesis during SARS-CoV infection remains unknown.

In conclusion, we demonstrate a crucial role for cooperation of antigen-specific antibodies and phagocytic cells (monocyte-derived infiltrating macrophages and partially alveolar macrophages) in the elimination of SARS-CoV in mouse models of infection. Our findings provide a better understanding of the mechanism(s) by which host defenses control SARS-CoV infection. Ideally, this information can contribute to the development of novel therapeutic protocols or treatments for SARS.

Materials and methods

Virus and cells

These studies used the SARS-CoV Vietnam/NB-04/2003 strain. This strain, originally isolated from a single patient's throat lavage, was kindly provided by Dr. Mai Quynh Le (Hong et al., 2004) and further subcultured in Vero E6 cells grown in MEM (Nissui Pharmaceutical Co. Ltd., Tokyo, Japan) containing 5% FCS. All work using SARS-CoV was performed in Biosafety Level 3 facilities by personnel wearing powered air-purifying respirators (Shigematsu Co., Ltd., Tokyo, Japan).

Mouse infection model

SCID mice (female, 7–8 weeks old) were purchased from CLEA Japan, Inc. (Tokyo, Japan). BALB/c mice (female, >6 months old and 6–7 weeks old) and nude mice (female, 6 weeks old) were purchased from SLC (Shizuoka, Japan). The IFN-γ deficient mouse (BALB/c background) was the kind gift of Prof. Iwakura (The Institute of Medical Science, The University of Tokyo and Tokyo University of Science). On study day 0, mice were inoculated i.n. with SARS-CoV at 1×10^5 $TCID_{50}$ (20 μL) per mouse. At serial time points, mice were sacrificed under anesthesia following terminal blood collection, and the lungs were recovered. Portions of the tissues were frozen immediately at −80 °C or fixed in 10% buffered formalin. Blood was used for the in vitro neutralization assays and adoptive transfer experiments. All animal experiments using mice were approved by the Animal Experiment Committee at The Institute of Medical Science, The University of Tokyo, and were performed in accordance with the animal experimentation guidelines of The Institute of Medical Science, The University of Tokyo.

Depletion of immunocompetent cells

To confirm the depletion efficacy of anti-CD4 mAb (GK1.5; 100 μL of ascites) or anti-CD8 mAb (53.6; 100 μL of ascites), BALB/c mice were injected i.v. with the indicated dose volumes. At 1 day after administration of the respective mAb, spleen-derived lymphocytes were analyzed by flow cytometry for expression of CD4 and CD8. To test efficacy against SARS-CoV infection, the anti-CD4 mAb and/or anti-CD8 mAb was injected i.v. on days −3, 0, +3 and +6 with respect to the SARS-CoV challenge. For experiments examining the depletion of $Gr\text{-}1^+$ ($Ly\text{-}6G^+$ and $Ly\text{-}6C^+$) cells, anti-Gr-1 mAb (250 μg, RB6-8C5; rat IgG2b) was injected i.p. 6 days after SARS-CoV challenge (Fujisawa, 2008). The hybridoma RB6-8C5 was obtained from the Cell Resource Center for Biomedical Research, Institute of Development, Aging, and Cancer, Tohoku University (Miyagi, Japan). Anti-IL2Rβ mAb (TM-β1), used for the depletion of NK cells (Tanaka et al., 1993), was the kind gift of Prof. Miyasaka (Osaka University, Japan). TM-β1 (100 μL of ascites) was injected i.p. 3 days before adoptive transfer of BALB/c mice splenocytes into both SCID and BALB/c mice. Anti-Ly6G mAb (1 mg, 1A8; rat IgG2a [purchased from Bio-XCell Co., Ltd.]) was injected i.p. 6 days after SARS-CoV challenge to deplete $Ly\text{-}6G^+$ cells (neutrophils) (Daley et al., 2008). The depletion of the respective immunocompetent cells was confirmed by flow cytometric analysis. One hundred microliters of 30% clodronate liposome

suspension was injected i.n. in mice 6 days after SARS-CoV challenge to deplete alveolar macrophages (Pribul et al., 2008). The numbers of AMs were quantified in the bronchoalveolar lavage fluid (BALF). To deplete complement, cobra venom factor (CVF; 40 U/mouse, a gift of Prof.Okada, Nagoya City University, Japan) was injected i.p. in SCID mice both 5 and 6 days after SARS-CoV challenge (Pleyer et al., 1992).

Adoptive transfer of immunocompetent cells

Splenocytes were isolated from SARS-CoV-infected (9 dpi; sensitized) or naïve BALB/c mice (over 6 months old); the resulting cells then were administered (at 4×10^7 cells/animal) to recipient naïve SCID mouse i.v. 1 day before challenge. Splenocytes from NK cell-depleted BALB/c mice also were administered to recipient NK cell-depleted SCID mice as described above. $CD4^+$ cells (1×10^7 cells) were isolated from the spleen of naïve BALB/c mice using anti-CD4 magnetic beads, followed by purification with an AutoMACS sorter (Miltenyi Biotech, Bergisch Gladbach, Germany). Isolated $CD4^+$ cells ($>96\%$ purity) were adoptively transplanted into each recipient naïve SCID or nude mouse. In addition, splenocytes of naïve BALB/c mice were divided into the $CD19^+$ cells (B cells) and residual cells ($CD19^-$ cells, including T cells) using anti-CD19 magnetic beads (Miltenyi Biotech). The B cells ($CD19^+$cells; 2×10^7 cells/mouse) and/or the residual cells ($CD19^-$ cells; 2×10^7 cells/mouse) then were adoptively transplanted into the recipient naïve SCID mice.

Passive transfer of antisera

In our previous study, New Zealand White rabbits were immunized with a recombinant vaccinia virus LC16m8 strain expressing the gene for the S protein of SARS-CoV (Kitabatake et al., 2007). The resulting antisera (rabbit anti-S protein) showed high neutralizing activity against SARS-CoV ($NT_{50} > 300$). As negative controls for this rabbit anti-S antiserum, we used normal rabbit serum and/or rabbit antiserum against vaccinia virus strain LC16m8. Mouse anti-SARS-CoV antiserum was obtained from BALB/c mice at 9 days after SARS-CoV infection, at which point the antiserum exhibited $NT_{50} = \sim 40$. For passive transfer, each recipient naïve mouse received 0.2–0.5 mL of rabbit anti-S protein antiserum or mouse anti-SARS-CoV antiserum, administered i.v. at 6 dpi (or at 6 and 8 dpi).

Determination of viral titers in the lung

The SARS-CoV titers in the murine lung were determined as described previously (Yasui et al., 2008). Briefly, lung tissue samples were homogenized in 10 volumes of Leibovitz 15 medium (Invitrogen, CA, USA). The homogenate was centrifuged at $400 \times g$ for 10 min at 4 °C. The supernatant was collected and stored at −80 °C until use. Serial 10-fold dilutions of the supernatant were added to Vero E6 cells seeded on 96-well plates. After 6 days of incubation, the cells were fixed with 10% buffered formalin. Viral titers were determined as the 50% endpoint dilution of the homogenate that induced the cytopathic effect, and were expressed as $TCID_{50}$ per gram of tissue. The method used for endpoint calculation was that described by Reed and Muench (1938).

In vitro neutralization assay for SARS-CoV

Serial 2-fold dilutions of heat-inactivated sera ($>1:4$) were mixed with equal volumes of 200 $TCID_{50}$ of SARS-CoV and incubated at 37 °C for 1 h. Vero E6 cells then were infected with 100 μL of the virus-serum mixtures in 96-well plates. After 6 days of incubation, the neutralization titer was determined as the endpoint dilution of the serum at which there was 50% inhibition of the SARS-CoV-induced cytopathic effect. The method used for endpoint calculation was that described by Reed and Muench (1938).

Lung histopathology and immunohistochemistry

In accordance with a previous report, 10% formalin-fixed lung tissues of the SARS-CoV-infected mice were embedded in paraffin (Yasui et al., 2008). Paraffin block sections (4-μm thickness) were stained with hematoxylin and eosin. Antigen retrieval was performed by autoclaving sections in 10 mM citrate buffer (pH 6.0) for 20 min, and then the sections were immersed in 3% hydrogen peroxide (H_2O_2) at room temperature (RT) for 5 min to inactivate endogenous peroxidase. The sections were blocked with 5% skim milk in Tris-buffered saline containing 0.1% Tween-20 at RT for 30 min, and then were incubated (overnight at 4 °C) with 1 μg/mL of anti-N protein of SARS-CoV polyclonal antibody (pAb) (IMG548; IMGENEX, San Diego, CA, USA). Secondary labeling was performed by incubation (at RT for 2 h) with 1:1000 donkey anti-rabbit IgG (GE Healthcare, Buckinghamshire, UK), followed by color development with 3,3'-diaminobenzidine in 50 mM Tris–HCl (pH 7.6) for 30 min. Nuclear staining was performed with hematoxylin solution. Slides were imaged using an Axio Imager A2 microscope (Carl Zeiss Inc., Oberkochen, Germany).

Extraction of total RNA and quantitative RT-PCR

Total RNA samples were extracted from lung using the illustra RNAspin Midi isolation kit (GE Healthcare) according to the manufacturer's instructions. Messenger RNA levels for the N protein-encoding gene of SARS-CoV were measured using the TaqMan EZ RT-PCT kit (Applied Biosystems, Branchburg, NJ, USA). Each 25 μL reaction mixture contained 5.0 μL 5× TaqMan EZ buffer, 3.0 μL 25 mM $Mn(OAc)_2$, 0.25 μL 1 U/μL AmpErase UNG (uracil N-glycosylase), 1.0 μL 2.5 U/μL of rTth DNA polymerase, 3.0 μL dNTP mix (10 mM dATP, 10 mM dCTP, 10 mM dGTP, and 20 mM dUTP), 0.25 μL 10 μM probe, 0.25 μL each 50 μM forward and reverse primers, 7.0 μL nuclease-free water, and 5.0 μL nucleic acid extract. Amplification was carried out in 96-well plates on the ABI Prism 7700 and Sequence Detection System software ver. 1.7. Thermocycling conditions consisted of 2 min at 50 °C for UNG treatment, 30 min at 60 °C for reverse transcription, 5 min at 95 °C for deactivation of UNG, and 50 cycles of 15 s at 95 °C and 1 min at 60 °C for amplification. Each run included pEFMyc-His-SARS-N plasmid (at 10^1, 10^2, 10^3, 10^4, 10^6, and 10^8 copies/5 μL) to provide a standard curve and at least one no-template control. The primers and probe used in this study were as follows: forward primer, 5'-GGAGCCTTGAATACACCCAAAG-3'; reverse primer, 5'-GCACGG-TGGCAGCATTG-3'; probe, 5'-(FAM)-CCACATTGGCACCCGCAATCC-(TAMRA)-3'.

Quantitation of complement C3 serum level

The depletion of complement was quantified by enzyme-linked immunosorbent assay (ELISA) for mouse complement C3 (Kamiya Biomedical Company, Seattle, WA, USA).

Statistical analysis

Data are presented as mean ± standard deviation (SD), where applicable. Inferential statistical analysis was performed by One-Way ANOVA, followed by Tukey's test. Non-parametric analysis was performed using the Kruskal–Wallis test, followed by Mann–Whitney's U test. A p value < 0.05 was considered statistically significant. All statistical calculations were performed with SPSS Statistics 17.0 software (SPSS Inc., Chicago, IL, USA).

Acknowledgments

We express our gratitude to Ms. Iyo Kataoka of the Institute of Medical Science, The University of Tokyo, for technical assistance in the evaluation of lung histopathology.

This study was supported in part by JSPS KAKENHI Grant number 21790455, the 21st Century Centers of Excellence (COE) Program on Global Strategies for Control of Tropical and Emerging Infectious Diseases at Nagasaki University, and by the Ministry of Education, Culture, Sports, Science, and Technology of Japan.

References

Appay, V., Zaunders, J.J., Papagno, L., Sutton, J., Jaramillo, A., Waters, A., Easterbrook, P., Grey, P., Smith, D., McMichael, A.J., Cooper, D.A., Rowland-Jones, S.L., Kelleher, A.D., 2002. Characterization of CD4+ CTLs ex vivo. J. Immunol. 168, 5954–5958.

Cameron, M.J., Ran, L., Xu, L., Danesh, A., Bermejo-Martin, J.F., Cameron, C.M., Muller, M.P., Gold, W.L., Richardson, S.E., Poutanen, S.M., Willey, B.M., DeVries, M.E., Fang, Y., Seneviratne, C., Bosinger, S.E., Persad, D., Wilkinson, P., Greller, L. D., Somogyi, R., Humar, A., Keshavjee, S., Louie, M., Loeb, M.B., Brunton, J., McGeer, A.J., Kelvin, D.J., 2007. Interferon-mediated immunopathological events are associated with atypical innate and adaptive immune responses in patients with severe acute respiratory syndrome. J. Virol. 81, 8692–8706.

Casazza, J.P., Betts, M.R., Price, D.A., Precopio, M.L., Ruff, L.E., Brenchley, J.M., Hill, B.J., Roederer, M., Douek, D.C., Koup, R.A., 2006. Acquisition of direct antiviral effector functions by CMV-specific CD4+ T lymphocytes with cellular maturation. J. Exp. Med. 203, 2865–2877.

Chen, J., Lau, Y.F., Lamirande, E.W., Paddock, C.D., Bartlett, J.H., Zaki, S.R., Subbarao, K., 2010. Cellular immune responses to severe acute respiratory syndrome coronavirus (SARS-CoV) infection in senescent BALB/c mice: CD4+ T cells are important in control of SARS-CoV infection. J. Virol. 84, 1289–1301.

Christensen, J.P., Cardin, R.D., Branum, K.C., Doherty, P.C., 1999. CD4+ T cell-mediated control of a gamma-herpesvirus in B cell-deficient mice is mediated by IFN-gamma. Proc.Natl. Acad. Sci. USA 96, 5135–5140.

Daley, J.M., Thomay, A.A., Connolly, M.D., Reichner, J.S., Albina, J.E., 2008. Use of Ly6G-specific monoclonal antibody to deplete neutrophils in mice. J. Leukoc. Biol. 83, 64–70.

Fan, Y.Y., Huang, Z.T., Li, L., Wu, M.H., Yu, T., Koup, R.A., Bailer, R.T., Wu, C.Y., 2009. Characterization of SARS-CoV-specific memory T cells from recovered individuals 4 years after infection. Arch. Virol. 154, 1093–1099.

Fowler, R.A., Lapinsky, S.E., Hallett, D., Detsky, A.S., Sibbald, W.J., Slutsky, A.S., Stewart, T.E., 2003. Critically ill patients with severe acute respiratory syndrome. J. Am. Med. Assoc. 290, 367–373.

Franks, T.J., Chong, P.Y., Chui, P., Galvin, J.R., Lourens, R.M., Reid, A.H., Selbs, E., McEvoy, C.P., Hayden, C.D., Fukuoka, J., Taubenberger, J.K., Travis, W.D., 2003. Lung pathology of severe acute respiratory syndrome (SARS): a study of 8 autopsy cases from Singapore. Hum. Pathol. 34, 743–748.

Fujisawa, H., 2008. Neutrophils play an essential role in cooperation with antibody in both protection against and recovery from pulmonary infection with influenza virus in mice. J. Virol. 82, 2772–2783.

Geissmann, F., Jung, S., Littman, D.R., 2003. Blood monocytes consist of two principal subsets with distinct migratory properties. Immunity 19, 71–82.

Ho, M.S., Chen, W.J., Chen, H.Y., Lin, S.F., Wang, M.C., Di, J., Lu, Y.T., Liu, C.L., Chang, S. C., Chao, C.L., King, C.C., Chiou, J.M., Su, I.J., Yang, J.Y., 2005. Neutralizing antibody response and SARS severity. Emerg. Infect. Dis. 11, 1730–1737.

Hong, T.C., Mai, Q.L., Cuong, D.V., Parida, M., Minekawa, H., Notomi, T., Hasebe, F., Morita, K., 2004. Development and evaluation of a novel loop-mediated isothermal amplification method for rapid detection of severe acute respiratory syndrome coronavirus. J. Clin. Microbiol. 42, 1956–1961.

Huang, K.J., Su, I.J., Theron, M., Wu, Y.C., Lai, S.K., Liu, C.C., Lei, H.Y., 2005. An interferon-gamma-related cytokine storm in SARS patients. J. Med. Virol. 75, 185–194.

Huber, V.C., Lynch, J.M., Bucher, D.J., Le, J., Metzger, D.W., 2001. Fc receptor-mediated phagocytosis makes a significant contribution to clearance of influenza virus infections. J. Immunol. 166, 7381–7388.

Iijima, N., Mattei, L.M., Iwasaki, A., 2011. Recruited inflammatory monocytes stimulate antiviral Th1 immunity in infected tissue. Proc. Natl. Acad. Sci. USA 108, 284–289.

Kam, Y.W., Kien, F., Roberts, A., Cheung, Y.C., Lamirande, E.W., Vogel, L., Chu, S.L., Tse, J., Guarner, J., Zaki, S.R., Subbarao, K., Peiris, M., Nal, B., Altmeyer, R., 2007. Antibodies against trimeric S glycoprotein protect hamsters against SARS-CoV challenge despite their capacity to mediate FcgammaRII-dependent entry into B cells in vitro. Vaccine 25, 729–740.

Kitabatake, M., Inoue, S., Yasui, F., Yokochi, S., Arai, M., Morita, K., Shida, H., Kidokoro, M., Murai, F., Le, M.Q., Mizuno, K., Matsushima, K., Kohara, M., 2007. SARS-CoV spike protein-expressing recombinant vaccinia virus efficiently induces neutralizing antibodies in rabbits pre-immunized with vaccinia virus. Vaccine 25, 630–637.

Landais, E., Saulquin, X., Scotet, E., Trautmann, L., Peyrat, M.A., Yates, J.L., Kwok, W. W., Bonneville, M., Houssaint, E., 2004. Direct killing of Epstein–Barr virus (EBV)-infected B cells by CD4 T cells directed against the EBV lytic protein BHRF1. Blood 103, 1408–1416.

Lee, N., Hui, D., Wu, A., Chan, P., Cameron, P., Joynt, G.M., Ahuja, A., Yung, M.Y., Leung, C.B., To, K.F., Lui, S.F., Szeto, C.C., Chung, S., Sung, J.J., 2003. A major outbreak of severe acute respiratory syndrome in Hong Kong. N. Engl. J. Med. 348, 1986–1994.

Li, C.K., Wu, H., Yan, H., Ma, S., Wang, L., Zhang, M., Tang, X., Temperton, N.J., Weiss, R.A., Brenchley, J.M., Douek, D.C., Mongkolsapaya, J., Tran, B.H., Lin, C.L., Screaton, G.R., Hou, J.L., McMichael, A.J., Xu, X.N., 2008. T cell responses to whole SARS coronavirus in humans. J. Immunol. 181, 5490–5500.

Lin, K.L., Suzuki, Y., Nakano, H., Ramsburg, E., Gunn, M.D., 2008. CCR2+ monocyte-derived dendritic cells and exudate macrophages produce influenza-induced pulmonary immune pathology and mortality. J. Immunol. 180, 2562–2572.

Luo, D., Ni, B., Zhao, G., Jia, Z., Zhou, L., Pacal, M., Zhang, L., Zhang, S., Xing, L., Lin, Z., Wang, L., Li, J., Liang, Y., Shi, X., Zhao, T., Zou, L., Wu, Y., Wang, X., 2007. Protection from infection with severe acute respiratory syndrome coronavirus in a Chinese hamster model by equine neutralizing F(ab')2. Vir. Immunol. 20, 495–502.

Nagata, N., Iwata, N., Hasegawa, H., Fukushi, S., Harashima, A., Sato, Y., Saijo, M., Taguchi, F., Morikawa, S., Sata, T., 2008. Mouse-passaged severe acute respiratory syndrome-associated coronavirus leads to lethal pulmonary edema and diffuse alveolar damage in adult but not young mice. Am. J. Pathol. 172, 1625–1637.

Nicholls, J.M., Poon, L.L., Lee, K.C., Ng, W.F., Lai, S.T., Leung, C.Y., Chu, C.M., Hui, P.K., Mak, K.L., Lim, W., Yan, K.W., Chan, K.H., Tsang, N.C., Guan, Y., Yuen, K.Y., Peiris, J.S., 2003. Lung pathology of fatal severe acute respiratory syndrome. Lancet 361, 1773–1778.

Peiris, J.S., Chu, C.M., Cheng, V.C., Chan, K.S., Hung, I.F., Poon, L.L., Law, K.I., Tang, B.S., Hon, T.Y., Chan, C.S., Chan, K.H., Ng, J.S., Zheng, B.J., Ng, W.L., Lai, R.W., Guan, Y., Yuen, K.Y., 2003a. Clinical progression and viral load in a community outbreak of coronavirus-associated SARS pneumonia: a prospective study. Lancet 361, 1767–1772.

Peiris, J.S., Yuen, K.Y., Osterhaus, A.D., Stohr, K., 2003b. The severe acute respiratory syndrome. N. Engl. J. Med. 349, 2431–2441.

Peiris, J.S., Guan, Y., Yuen, K.Y., 2004. Severe acute respiratory syndrome. Nat. Med. 10, S88–S97.

Pleyer, U., Mondino, B.J., Sumner, H.L., 1992. The effect of systemic decomplementation with cobra venom factor on corneal complement levels in guinea pigs. Invest. Ophthalmol. Vis. Sci. 33, 2212–2215.

Pribul, P.K., Harker, J., Wang, B., Wang, H., Tregoning, J.S., Schwarze, J., Openshaw, P. J., 2008. Alveolar macrophages are a major determinant of early responses to viral lung infection but do not influence subsequent disease development. J. Virol. 82, 4441–4448.

Reed, L.J., Muench, H., 1938. A simple method of estimating fifty percent endpoints. Am. J. Hyg. 27, 493–497.

Roberts, A., Paddock, C., Vogel, L., Butler, E., Zaki, S., Subbarao, K., 2005. Aged BALB/c mice as a model for increased severity of severe acute respiratory syndrome in elderly humans. J. Virol. 79, 5833–5838.

Roberts, A., Deming, D., Paddock, C.D., Cheng, A., Yount, B., Vogel, L., Herman, B.D., Sheahan, T., Heise, M., Genrich, G.L., Zaki, S.R., Baric, R., Subbarao, K., 2007. A mouse-adapted SARS-coronavirus causes disease and mortality in BALB/c mice. PLoS Pathog. 3, e5.

Rockx, B., Corti, D., Donaldson, E., Sheahan, T., Stadler, K., Lanzavecchia, A., Baric, R., 2008. Structural basis for potent cross-neutralizing human monoclonal antibody protection against lethal human and zoonotic severe acute respiratory syndrome coronavirus challenge. J. Virol. 82, 3220–3235.

Rockx, B., Donaldson, E., Frieman, M., Sheahan, T., Corti, D., Lanzavecchia, A., Baric, R.S., 2011. Escape from human monoclonal antibody neutralization affects in vitro and in vivo fitness of severe acute respiratory syndrome coronavirus. J. Infect. Dis. 201, 946–955.

Stockman, L.J., Massoudi, M.S., Helfand, R., Erdman, D., Siwek, A.M., Anderson, L.J., Parashar, U.D., 2007. Severe acute respiratory syndrome in children. Pediatr. Infect. Dis. J. 26, 68–74.

Subbarao, K., McAuliffe, J., Vogel, L., Fahle, G., Fischer, S., Tatti, K., Packard, M., Shieh, W.J., Zaki, S., Murphy, B., 2004. Prior infection and passive transfer of neutralizing antibody prevent replication of severe acute respiratory syndrome coronavirus in the respiratory tract of mice. J. Virol. 78, 3572–3577.

Tanaka, T., Kitamura, F., Nagasaka, Y., Kuida, K., Suwa, H., Miyasaka, M., 1993. Selective long-term elimination of natural killer cells in vivo by an anti-interleukin 2 receptor beta chain monoclonal antibody in mice. J. Exp. Med. 178, 1103–1107.

Temperton, N.J., Chan, P.K., Simmons, G., Zambon, M.C., Tedder, R.S., Takeuchi, Y., Weiss, R.A., 2005. Longitudinally profiling neutralizing antibody response to SARS coronavirus with pseudotypes. Emerg. Infect. Dis. 11, 411–416.

Tumpey, T.M., Garcia-Sastre, A., Taubenberger, J.K., Palese, P., Swayne, D.E., Pantin-Jackwood, M.J., Schultz-Cherry, S., Solorzano, A., Van Rooijen, N., Katz, J.M., Basler, C.F., 2005. Pathogenicity of influenza viruses with genes from the 1918 pandemic virus: functional roles of alveolar macrophages and neutrophils in limiting virus replication and mortality in mice. J. Virol. 79, 14933–14944.

Varol, C., Yona, S., Jung, S., 2009. Origins and tissue-context-dependent fates of blood monocytes. Immunol. Cell Biol. 87, 30–38.

Wang, J.T., Chang, S.C., 2004. Severe acute respiratory syndrome. Curr. Opin. Infect. Dis. 17, 143–148.

Wong, C.K., Lam, C.W., Wu, A.K., Ip, W.K., Lee, N.L., Chan, I.H., Lit, L.C., Hui, D.S., Chan, M.H., Chung, S.S., Sung, J.J., 2004. Plasma inflammatory cytokines and chemokines in severe acute respiratory syndrome. Clin. Exp. Immunol. 136, 95–103.

Yang, L., Peng, H., Zhu, Z., Li, G., Huang, Z., Zhao, Z., Koup, R.A., Bailer, R.T., Wu, C., 2007. Persistent memory CD4+ and CD8+ T-cell responses in recovered severe

acute respiratory syndrome (SARS) patients to SARS coronavirus M antigen. J. Gen. Virol. 88, 2740–2748.
Yang, L.T., Peng, H., Zhu, Z.L., Li, G., Huang, Z.T., Zhao, Z.X., Koup, R.A., Bailer, R.T., Wu, C.Y., 2006. Long-lived effector/central memory T-cell responses to severe acute respiratory syndrome coronavirus (SARS-CoV) S antigen in recovered SARS patients. Clin. Immunol. 120, 171–178.
Yang, Z.Y., Kong, W.P., Huang, Y., Roberts, A., Murphy, B.R., Subbarao, K., Nabel, G.J., 2004. A DNA vaccine induces SARS coronavirus neutralization and protective immunity in mice. Nature 428, 561–564.
Yasui, F., Kai, C., Kitabatake, M., Inoue, S., Yoneda, M., Yokochi, S., Kase, R., Sekiguchi, S., Morita, K., Hishima, T., Suzuki, H., Karamatsu, K., Yasutomi, Y., Shida, H., Kidokoro, M., Mizuno, K., Matsushima, K., Kohara, M., 2008. Prior immunization with severe acute respiratory syndrome (SARS)-associated coronavirus (SARS-CoV) nucleocapsid protein causes severe pneumonia in mice infected with SARS-CoV. J. Immunol. 181, 6337–6348.
Zhao, J., Perlman, S., 2010. T cell responses are required for protection from clinical disease and for virus clearance in severe acute respiratory syndrome coronavirus-infected mice. J. Virol. 84, 9318–9325.
Zhao, J., Van Rooijen, N., Perlman, S., 2009. Evasion by stealth: inefficient immune activation underlies poor T cell response and severe disease in SARS-CoV-infected mice. PLoS Pathog. 5, e1000636.
Zhao, J., Zhao, J., Legge, K., Perlman, S., 2011. Age-related increases in PGD(2) expression impair respiratory DC migration, resulting in diminished T cell responses upon respiratory virus infection in mice. J. Clin. Invest. 121, 4921–4930.
Zhao, J., Wohlford-Lenane, C., Zhao, J., Fleming, E., Lane, T.E., McCray , P.B., Perlman, S., 2012. Intranasal treatment with poly(I-C) protects aged mice from lethal respiratory virus infections. J. Virol. 86, 11416–11424.
Zhu, Z., Chakraborti, S., He, Y., Roberts, A., Sheahan, T., Xiao, X., Hensley, L.E., Prabakaran, P., Rockx, B., Sidorov, I.A., Corti, D., Vogel, L., Feng, Y., Kim, J.O., Wang, L.F., Baric, R., Lanzavecchia, A., Curtis, K.M., Nabel, G.J., Subbarao, K., Jiang, S., Dimitrov, D.S., 2007. Potent cross-reactive neutralization of SARS coronavirus isolates by human monoclonal antibodies. Proc. Natl. Acad. Sci. USA 104, 12123–12128.

The American Journal of Pathology, Vol. 184, No. 1, January 2014

ELSEVIER

The American Journal of
PATHOLOGY

ajp.amjpathol.org

CARDIOVASCULAR, PULMONARY, AND RENAL PATHOLOGY

Histopathological Evaluation of the Diversity of Cells Susceptible to H5N1 Virulent Avian Influenza Virus

Haru Ogiwara,* Fumihiko Yasui,* Keisuke Munekata,* Asako Takagi-Kamiya,* Tsubasa Munakata,* Namiko Nomura,† Futoshi Shibasaki,† Kazuhiko Kuwahara,‡ Nobuo Sakaguchi,§ Yoshihiro Sakoda,§ Hiroshi Kida,§ and Michinori Kohara*

From the Departments of Microbiology and Cell Biology and Molecular Medical Research,† Tokyo Metropolitan Institute of Medical Science, Tokyo; the Department of Immunology,‡ Graduate School of Life Sciences, Kumamoto University, Kumamoto; and the Laboratory of Microbiology,§ Graduate School of Veterinary Medicine, Hokkaido University, Sapporo, Japan*

Accepted for publication October 3, 2013.

Address correspondence to Michinori Kohara, Ph.D., Department of Microbiology and Cell Biology, Tokyo Metropolitan Institute of Medical Science, 2-1-6 Kami-kitazawa, Setagaya-ku, Tokyo 156-8506, Japan. E-mail: kohara-mc@igakuken.or.jp.

Patients infected with highly pathogenic avian influenza A H5N1 viruses (H5N1 HPAIV) show diffuse alveolar damage. However, the temporal progression of tissue damage and repair after viral infection remains poorly defined. Therefore, we assessed the sequential histopathological characteristics of mouse lung after intranasal infection with H5N1 HPAIV or H1N1 2009 pandemic influenza virus (H1N1 pdm). We determined the amount and localization of virus in the lung through IHC staining and *in situ* hybridization. IHC used antibodies raised against the virus protein and antibodies specific for macrophages, type II pneumocytes, or proliferating cell nuclear antigen. *In situ* hybridization used RNA probes against both viral RNA and mRNA encoding the nucleoprotein and the hemagglutinin protein. H5N1 HPAIV infection and replication were observed in multiple lung cell types and might result in rapid progression of lung injury. Both type II pneumocytes and macrophages proliferated after H5N1 HPAIV infection. However, the abundant macrophages failed to block the viral attack, and proliferation of type II pneumocytes failed to restore the damaged alveoli. In contrast, mice infected with H1N1 pdm exhibited modest proliferation of type II pneumocytes and macrophages and slight alveolar damage. These results suggest that the virulence of H5N1 HPAIV results from the wide range of cell tropism of the virus, excessive virus replication, and rapid development of diffuse alveolar damage. *(Am J Pathol 2014, 184: 171–183; http://dx.doi.org/10.1016/j.ajpath.2013.10.004)*

Seasonal, pandemic, and zoonotic influenza A virus infections show substantial morbidity and mortality in humans. Seasonal influenza A virus infections in humans are usually mild and cause pneumonia only in a few infected individuals. Pandemic influenza virus infections vary in their disease outcome. Zoonotic influenza virus infections in humans vary from self-limiting conjunctivitis to severe, often fatal, pneumonia. Highly pathogenic avian influenza H5N1 virus (H5N1 HPAIV), implicated in poultry outbreaks,[1,2] can be transmitted zoonotically to humans, as has been observed in areas of Asia and Africa.[3–5] Fatal outcomes have been reported at approximately 60% in the sporadic transmission of this avian influenza H5N1 virus to humans.[5–7] There is no evidence that the avian influenza virus has become efficiently transmissible among humans, a change that could result in a new pandemic.[8]

The outcome after infection with influenza virus can range from slight to severe illness, depending on the kinds of cells that are affected during lung tissue infection.[9–11] Events occurring early in infection determine the extent of damage, which can range from bronchitis to pneumonia. In the most severe cases, diffuse alveolar damage (DAD) may be induced during the early stages, and healing and/or scarring may ensue, depending on the persistence of disease. Occasionally, bacterial infection also may occur, with associated effects expressed mainly in the later stages of the disease. Pathological damage caused by influenza viruses in humans and in animal models depends on the virulence of

Supported by grants from the Ministry of Education, Culture, Sports, Science and Technology of Japan; the Program for Promotion of Fundamental Studies in Pandemic Influenza of the Tokyo Metropolitan Institute of Medical Science of Japan; and the Ministry of Health, Labour and Welfare of Japan.

Current address of N.N., RIKEN Center for Integrative Medical Sciences, Kanagawa, Japan.

http://dx.doi.org/10.1016/j.ajpath.2013.10.004

the infective agent and on the host response. All influenza viruses infect the respiratory tract epithelium from the nasal passages to the bronchioles; however, highly virulent viruses (eg, H1N1 1918 and H5N1 HPAIV) tend to infect pneumocytes and resident macrophages in the alveoli. In susceptible individuals, inflammation of the alveolar walls results in DAD. In contrast, low-virulence viruses (seasonal H1N1) primarily cause inflammation, congestion, and epithelial necrosis of the trachea, bronchi, and bronchioles. Tissue tropism is an important factor, and depends largely on the ability of the virus to attach to the host cell.[12–14] We investigated virus replication and histopathological progression of lung tissue in mice infected with H5N1 HPAIV, particularly focusing on the lower respiratory tract and alveoli, with direct comparison to the histopathological characteristics of mice infected with H1N1 pandemic (pdm) influenza virus 2009 virus.

Materials and Methods

Viruses

This study used the H5N1 highly pathogenic avian influenza virus A/whooper swan/Hokkaido/1/2008 strain (H5N1 HPAIV) and the H1N1 pandemic influenza virus A/Tokyo/2619/2009 strain (H1N1 pdm 2009). All experiments using H5N1 HPAIV were performed in biosafety level 3 facilities. H5N1 HPAIV was propagated in embryonated eggs. Virus-containing allantoic fluid was harvested and stored in aliquots at −80°C pending use. H1N1 pdm 2009 virus was subcultured in MDCK cells grown in modified Eagle's medium (MEM; Nissui Pharmaceutical Co Ltd, Tokyo, Japan) containing 1% bovine serum albumin and 10 μg/mL acetyl-trypsin.

Antibodies

The monoclonal antibody (mAb) 8C1 (IgG1 κ), raised against mouse-derived influenza A H5N1 hemagglutinin (H5N1-HA), was established in this study by using GANP mouse.[15] This mAb was purified as the IgG fraction (0.86 mg/mL) using protein G column chromatography. Mouse mAb against the influenza A nucleoprotein (NP) was obtained from hybridoma HB-65, which was purchased from ATCC (Manassas, VA).[16,17] Mouse mAb was purified as the IgG fraction (1.64 mg/mL) using protein G column chromatography.

Infection of BALB/c Mice with Influenza Virus

All experimental animal protocols were approved by the Animal Use and Care Committee of Tokyo Metropolitan Institute of Medical Science (Tokyo, Japan). BALB/c mice (12- to 13-week-old females) were purchased from SLC (Shizuoka, Japan). For infection, animals were anesthetized by i.p. injection of 0.15 mL of ketamine/xylazine, and administered intranasally with 50 μL per mouse of infectious virus [2×10^6 plaque-forming units (PFUs) H1N1 pdm 2009 virus or 1×10^4 PFUs H5N1 HPAIV] diluted in vehicle (MEM medium containing 1% bovine serum albumin and MEM vitamin solution). An equivalent volume of vehicle was administered intranasally to each of the mice of the control group. At 1, 3, 6, or 7, and 9 days after infection, three to four mice per group were euthanized under deep anesthesia, and the lungs were collected. Segments of the lung tissues were frozen at −80°C or fixed in 10% buffered formalin.

Titration of Influenza Virus in the Lung Tissues

The left upper lung from each mouse was used for titration of influenza virus. The viral contents of the lung tissues were determined in three to four mice per time point in each group. Briefly, lung tissues were homogenized in nine volumes of Leibovitz 15 medium (Invitrogen, Carlsbad, CA). The homogenate was centrifuged at $3000 \times g$ for 10 minutes at 4°C. The supernatant was collected and stored at −80°C pending use. Serial 10-fold dilutions of the supernatant were added to MDCK cells seeded on 6-well plates. After 3 days of incubation, the cells were fixed with 10% buffered formalin. Viral titers were determined as plaque numbers resulting from added supernatant, and were expressed as PFUs per gram of tissue.

Histopathological Characteristics

The right lung lobe from each mouse was fixed in 10% buffered formalin, embedded in paraffin, divided into tissue sections (3 μm thick), stained with H&E, and subjected to routine histological examination. Histological changes were evaluated according to the modified methods of Trias et al,[18] van Riel et al,[9] or Vincent et al.[19] For each lung tissue section, 10 randomly selected microscopic fields were scanned at a magnification of ×100, and each field was graded visually on a scale from 0 to 7. The grading system for histological changes is defined as follows: 0, normal lung; 1, mild destruction of epithelium in trachea and bronchus; 2, mild infiltration of inflammatory cells around the periphery of bronchioles; 3, moderate infiltration of inflammatory cells around the alveolar walls, resulting in alveolar thickening; 4, mild alveolar injury accompanied by vascular damage of ≤10%; 5, moderate alveolar and vascular injury (11% to approximately 30%); 6, severe alveolar injury with hyaline membrane–associated alveolar hemorrhage of 31% to approximately 50%; and 7, severe alveolar injury with hyaline membrane–associated alveolar hemorrhage of ≥51%. The mean value of the grades obtained for all fields then was used as the grade of visual lung injury.

IHC for Viral Antigens

The formalin-fixed, paraffin-embedded tissue specimens described in the previous paragraph were divided into tissue sections (6 μm thick) and processed for immunohistochemical (IHC) studies. Influenza A viral NP or H5N1 hemagglutinin

(H5N1-HA) was detected/localized in lung tissue (after infection by the respective virus) using the Vector M.O.M. Immunodetection PK-2200 peroxidase kit (Vector Laboratories Inc., Burlingame, CA). After deparaffinization of tissue, slides were immersed in sodium citrate buffer, pH 6.0, and autoclaved at 120°C for 5 minutes. Sections were then treated with 3% hydrogen peroxide and blocked with blocking reagent. We used mouse anti-influenza NP mAb (HB65) at 1:1000 dilution (1.64 μg/mL) or anti–H5N1-HA mAb (8C1) at 1:2000 dilution (0.43 μg/mL) as the primary antibody, and biotinylated anti-mouse IgG polyclonal Ab at 1:250 dilution as the secondary antibody. After washing with PBS(-), slides were incubated in freshly complexed avidin-biotin hydroperoxidase reagent (Vector Laboratories, Inc.). Color development was performed with diaminobenzidine (Dojindo Laboratories, Kumamoto, Japan)/H_2O_2 solution, and sections were counterstained with hematoxylin. Stained sections were observed using an A2 upright microscope (Carl Zeiss Microimaging Co, Ltd, Göttingen, Germany), and images were captured using a ZEISS Axio Imager (Carl Zeiss Microimaging Co, Ltd). Positive expression of NP or H5N1-HA was evaluated and scored using the following IHC scoring system: 0, no positive cells; 1, rare positive cells; 2, infrequent positive cells; 3, common positive cells; and 4, extensive positive cells.[20]

IHC for Proliferating Alveolar Macrophages and Pneumocytes

To study the responses of type II pneumocytes and macrophages in the alveoli to H5N1 HPAIV infection, a double immune-staining technique was performed using two antibodies. The first antibody [mouse anti–proliferating cell nuclear antigen (PCNA) mAb; Beckman Coulter, Inc., Marseille, France] had specificity against the PCNA. The second antibody recognized a cell type–specific marker indicative of macrophages [ionized calcium-binding adapter molecular 1 (Iba1): polyclonal rabbit anti-Iba1 antibody; Wako Pure Chemical Industries, Ltd, Osaka, Japan] or type II pneumocytes [surfactant-associated protein C (SP-C): polyclonal rabbit anti–SP-C antibody; Santa Cruz Biotechnology, Santa Cruz, CA]. Staining (30 minutes, room temperature) was performed using the combination of anti-PCNA and anti-Iba1 or of anti-PCNA and anti–SP-C (each at 1:200 dilution) as the primary antibody. A biotin-conjugated anti-mouse IgG or an alkaline phosphatase–labeled donkey anti-rabbit IgG (Thermo Scientific, Waltham, MA) was used as the secondary Ab. For the detection of PCNA, the Vector PK-2200 peroxidase kit and freshly complexed avidin-biotin reagent were used (Bio-Rad Laboratories, Hercules, CA). Immunoreactants were visualized using a diaminobenzidine and 5-bromo-4-chloro-3-indolyl phosphate/nitro blue tetrazolium substrate system (1-StepTMNBT/BCIP plus Suppressor; Pierce Biotechnology, Thermo Scientific). Proliferation of alveolar epithelial cells or macrophages was assessed semiquantitatively, as follows. Each lung section was quantified in 10 randomly selected microscopic fields (magnification ×400). The proliferation index was defined as the mean percentage of PCNA-positive cells in SP-C–positive cells or in Iba1-positive cells.[21]

Cytokine and Chemokine Profiles

Samples of mouse lung were homogenized in a solution of 50 mmol/L Tris-HCl, pH 7.5, 150 mmol/L NaCl, 1.0% Triton X-100, and 20 mmol/L EDTA containing protease inhibitor.[22] The resulting homogenates were assessed for cytokines and chemokines using Bio-Plex cytokine assay kits (Bio-Rad Laboratories), according to the manufacturer's instructions. Specifically, we used the Bio-Plex mouse cytokine 23-Plex Panel, which includes 23 cytokines [IL-1α, IL-1β, IL-2, IL-3, IL-4, IL-5, IL-6, IL-9, IL-10, IL-12 (P40), IL-12 (P70), IL-13, IL-17, eotaxin, granulocyte colony-stimulating factor (G-CSF), granulocyte-macrophage colony-stimulating factor, interferon (IFN)-γ, keratinocyte-derived chemokine, monocyte chemotactic protein (MCP)-1, macrophage inflammatory protein (MIP)-1α, MIP-1β, regulated on activation normal T cell expressed and secreted, and tumor necrosis factor (TNF)-α], and the Bio-Plex mouse cytokine 9-Plex Panel, which includes nine cytokines (IL-15, IL-18, fibroblastic growth factor-basic, leukemia inhibitory factor, macrophage colony-stimulating factor, monokine induced by IFN-γ, MIP-2, platelet-derived growth factor-β, and vascular endothelial growth factor). Samples were analyzed on a Bio-Rad 96-well plate reader using the Bio-Plex Suspension Array System and Bio-Plex Manager software version 5.0 (Bio-Rad Laboratories). We also measured protein levels in the lung homogenates using the DC protein assay kit (Bio-Rad Laboratories), according to the manufacturer's instructions. The concentrations of cytokines in the lung tissues were calculated as pg cytokine/mg total protein in the lung homogenates.

In Vitro Transcription of the RNA Probes

Full-length NP- and HA-encoding cDNAs (from H5N1 HPAIV or H1N1 pdm 2009 virus) were cloned in either orientation under control of a T7 promoter. The (+)- or (−)-strand synthetic RNAs for the genes were transcribed and labeled using the digoxigenin (DIG) RNA labeling kit (SP6/T7) (Roche Diagnostics, GmbH, Mannheim, Germany), according to the manufacturer's instructions. RNA products were purified over a G-50 column, precipitated with ethanol, and resuspended in 10 mmol/L Tris and 1 mmol/L EDTA, pH 7.4 ($T_{10}E_1$). The resulting suspensions were assayed for RNA concentration, and the length of each synthetic RNA was confirmed by 1.5% formaldehyde denaturation gel electrophoresis. The labeled transcripts were hydrolyzed with carbonic acid buffer (pH 10.2) to yield RNA fragments of approximately 150 bp in length. A hydrolyzed probe was precipitated with ethanol and resuspended in RNase-free water. The resulting suspensions were again

assayed for RNA concentration, and the length of each synthetic RNA was confirmed by 2.0% formaldehyde denaturation gel electrophoresis.[23]

In Situ Hybridization Analysis

The lung tissue samples for NP and HA RNA detection were fixed in 10% buffered formalin (pH 7.4), embedded in paraffin, and cut into sections (6 μm thick). The slide-mounted sections were washed three times (8 minutes per wash) in xylene, three times (5 minutes per wash) in 99.5% ethanol, and three times (5 minutes per wash) in 75% ethanol, then rehydrated in distilled water for deparaffinization. The tissue slides were treated with 30 μg/mL proteinase K for 30 minutes at 37°C. After washing the tissue samples twice with diethyl pyrocarbonate–treated PBS at room temperature, the tissue samples were incubated in 95% formamide and 0.1× standard saline citrate (SSC; 1× SSC: 150 mmol/L NaCl and 15 mmol/L sodium citrate) for 15 minutes at 65°C. After chilling on ice, the slides were incubated in 100 μL of prehybridization solution for 60 minutes at room temperature. Prehybridization solution was composed of 50% formamide, 2× SSC, 1 μg/mL of salmon sperm DNA, 1 μg/mL of yeast tRNA, and 2 mmol/L vanadyl ribonucleoside complex. Then, the slides were incubated in 25 μL of hybridization solution (prehybridization solution containing 10% dextran sulfate and 200 ng/mL of the RNA probes) for 18 hours at 42°C. After hybridization, the slides were washed three times with solution 1 (50% formamide and 2× SSC at pH 7.4) for 20 minutes at 50°C. The tissue sections then were treated with 1 μg/mL RNase A for 10 minutes at 37°C in PBS and washed three times in wash solution 2 (0.1× SSC at pH 7.4) for 20 minutes at 50°C. Next, the tissue sections were incubated in blocking solution (Roche blocking reagent) for 30 minutes at room temperature. To detect DIG-labeled probe, an alkaline phosphatase–labeled sheep anti-DIG antibody (Roche) was used as the primary antibody. The slides then were incubated in 25 μL dye solution [338 μg/mL nitroblue tetrazolium chloride, 175 μg/mL 5-bromo-4-chloro-3-indolyl-phosphate, 4-toluidine salt, and 1 mmol/L levamisole (Vector Laboratories Inc.) in 100 mmol/L Tris-HCl (pH 9.5), 100 mmol/L NaCl, and 50 mmol/L $MgCl_2$] for 12 hours at room temperature in the dark. Stained sections were observed using an A2 upright microscope (Carl Zeiss Microimaging Co, Ltd), and images were captured using a ZEISS Axio Imager.

Results

Replication of Influenza Viruses

The titer of H5N1 HPAIV in lung tissues increased approximately 200-fold over the first 6 days after infection, before subsequently decreasing (Figure 1A). In contrast, the titer in lung tissue after H1N1 pdm 2009 virus infection progressively decreased until the last detection on 7 days after infection (Figure 1B). This distinction was observed despite the higher infecting titer used with H1N1 pdm 2009 virus (2×10^6 PFUs) compared with H5N1 HPAIV (1×10^4 PFUs). Consistent with the observed lung titers, all of the mice ($n = 4$) infected with H1N1 pdm 2009 virus survived for 9 days, whereas only 29% ($n = 2$ of 7) of H5N1 HPAIV-infected mice survived over the same interval.

Evaluation of Lung Histopathological Characteristics

Owing to the remarkable viral expansion, tissue damage extended rapidly to the lower respiratory tract within 3 days in mice infected with H5N1 HPAIV. Three days after infection, various degrees of bronchitis and epithelial necrosis were observed (Figure 1C). Interstitial inflammation, hyaline layer formation, varying degrees of alveolar edema, hemorrhage, and inflammation also were observed (Figure 1C). Furthermore, alveolar collapse and DAD were observed 9 days after infection. In contrast, histopathological observation of the lungs from mice infected with H1N1 pdm 2009 virus revealed that inflammation was restricted, detected primarily in bronchioles and occasional alveoli (Figure 1D). Consistent with these observations, histopathological scores were elevated more than twofold in the lungs of mice infected with H5N1 HPAIV compared with those of mice infected with H1N1 pdm 2009 virus (Figure 1, E and F).

Localization of Viral Antigens in Lung Tissue

To further characterize the intensely damaged lung tissues of mice infected with H5N1 HPAIV, we investigated the production of viral proteins in various lung cell types. NP antigen was detected in bronchial epithelial cells, type II pneumocytes, macrophages, vascular endothelium, and perivascular lymphocytes (Figure 2A). High levels of NP antigen also were seen in necrotic materials associated with the respiratory tract (Figure 2A). Expression of NP antigen exhibited a time-dependent expansion to the alveoli and vascular endothelium; expression in the bronchus gradually faded from day 3 to day 9 after infection (Figure 2, A and B).

In mice infected with H1N1 pdm 2009 virus, NP antigen was detected predominantly in the epithelial cells of the bronchus and bronchiole (Figure 2, C and D). The levels of NP antigen in endothelial cells, vascular and perivascular lymphocytes (Figure 2, C and D), and alveoli (Figure 2, C and D) remained low compared with the levels of NP antigen seen in mice infected with H5N1 HPAIV (Figure 2, A and B). These results suggested that H1N1 pdm 2009 virus expansion in the lung tissue was limited, occurring mainly in epithelial cells of the bronchus and bronchiole; antigen detection showed limited induction in the alveoli (Figure 2, C and D), in contrast to the pattern seen in mice infected with H5N1 HPAIV (Figure 2, A and B).

We further studied the IHC staining for NP antigen or H5N1-HA antigen using a mouse monoclonal antibody that was generated (for this study) by using GANP Tg mouse; staining was performed with the respective antibodies on

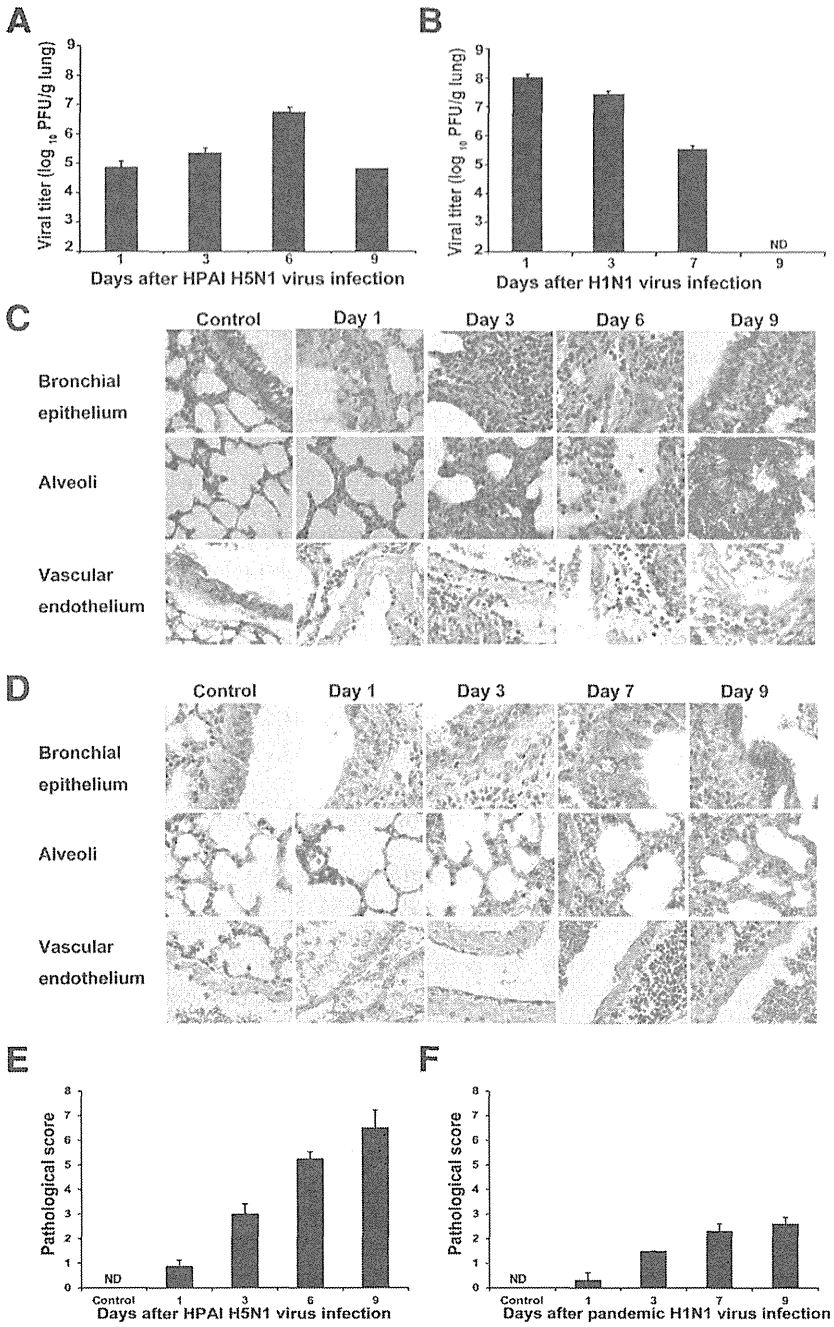

Figure 1 Pneumonia progression in mice after intranasal infection with H5N1 HPAIV or influenza A/H1N1 pdm 2009 virus. **A** and **B**: The virus titer of lung tissue was determined in three to four mice at each time point after intranasal infection with H5N1 HPAIV (1, 3, 6, and 9 days after infection; **A**) and with H1N1 pdm 2009 (1, 3, 7, and 9 days after infection; **B**). **C** and **D**: Lung histopathological characteristics were evaluated at different levels of the lower respiratory tract after infection with H5N1 HPAIV (**C**) or with H1N1 pdm 2009 virus (**D**). Representative figures at each time point (three to four mice per time point) are shown, with the three rows of images in both **C** and **D** corresponding to bronchial epithelium, alveoli, and vascular endothelium. Original magnification, ×630. Mice administered with vehicle were used as a control group. **E** and **F**: Pathological score of the lungs obtained from mice infected with influenza H5N1 HPAIV (**E**) and pandemic H1N1 virus (**F**). Scoring of the lung histological characteristics was done in three to four mice from each group at each time point. Data are expressed as means ± SD. ND, not detected.

paired serial sections of lung tissue obtained 3 days after infection with H5N1 HPAIV. Staining for H5N1-HA antigen achieved a higher intensity than that seen for NP antigen (Figure 3A). Thus, H5N1-HA antigen may provide improved sensitivity for detection of H5N1 HPAIV-infected lung tissue (Figure 3, B and C).

Detection of Viral RNA in Lung Tissue after Influenza Virus Infection

To evaluate viral replication in murine lung after influenza virus infection, we performed *in situ* hybridization with DIG-labeled RNA probes specific for either minus-strand RNA [viral RNA (vRNA)] or plus-strand RNA (mRNA) derived from influenza virus. We generated strand-specific (vRNA and mRNA) DIG-labeled RNA probes corresponding to the genes encoding HA and NP proteins, and confirmed the specificity of these probes in influenza virus–infected MDCK cells (Supplemental Figure S1). DIG-labeled RNA probes specific for the vRNA of either the HA- or NP-encoding genes stained the nuclei of MDCK cells infected with either H5N1 virus or H1N1 pdm 2009 virus. On the other hand, DIG-labeled RNA probes specific for the mRNA of either the HA- or NP-encoding genes

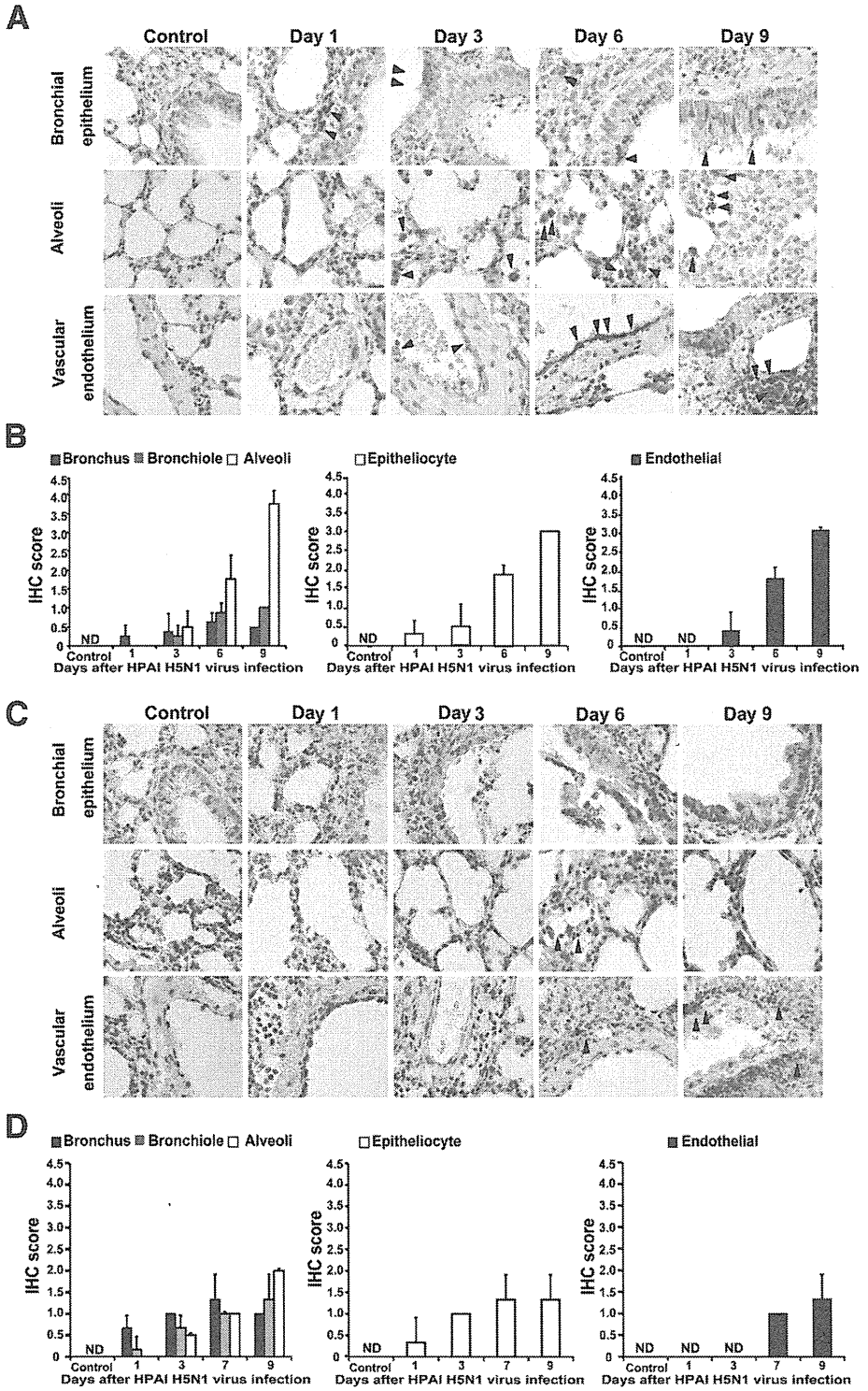

Figure 2 IHC analysis for NP protein in the lung of mice infected with H5N1 HPAIV or H1N1 pdm 2009 virus. IHC staining for NP protein was performed in the lungs of mice infected with H5N1 HPAIV (**A** and **B**) or H1N1 pdm 2009 virus (**C** and **D**). Mice administered vehicle were used as a control group. **A** and **C**: The expression of the NP protein is indicated (brown). **Arrowheads** indicate NP-positive cells. Each column of images indicates postinfection days 1 to 9. Representative figures at each time point (four mice per time point) are shown, with the three rows of images in both **A** and **C** corresponding to bronchial epithelium, alveoli, and vascular endothelium. Original magnification, ×630. **B** and **D**: Temporal changes in the numbers of NP-positive cells in the lung tissue of infected mice. Quantification of cells staining positive for NP protein in bronchus, bronchiole, alveoli, epithelial cells of lower respiratory tract, and vascular endothelium. Numbers of NP-positive cells were evaluated using the IHC scoring system (see *Materials and Methods*). Data are expressed as means ± SD of three to four mice per time point. ND, not detected.